A Diagnostic Analysis of the Presidents' Day Storm of February 1979

LANCE F. BOSART AND SONG C. LIN

State University of New York at Albany, Albany, NY 12222

(Manuscript received 22 August 1983, in final form 26 July 1984)

ABSTRACT

A diagnostic analysis of the Presidents' Day storm of February 1979 is used to extend and quantify earlier findings of Bosart. The initial growth of cyclonic vorticity in the lower troposphere is driven primarily by convergence along the Carolina coastal front. Rapid cyclone spinup accompanies the approach of a potent midtropospheric short wave trough from the Ohio Valley. An analysis of the vorticity structure discloses that cyclone spinup is enhanced by the vertical advection of vorticity in the strongly cyclonic *in situ* vorticity environment along the coast as the upper level trough overspreads the region. Similarly, a downward extension of high semigeostrophic potential vorticity air accompanies a tropopause fold to the west of the cyclone and prior to the rapid cyclogenesis stage, confirming a result of Uccellini and others. Semigeostrophic potential vorticity is poorly conserved, however, and there is evidence for a separate region of semigeostrophic potential vorticity growth below 800 mb near the coast.

Boundary layer warming and moistening approaches 400 and 1200 W m^{-2}, respectively, in the coastal waters of the precyclogenetic environment. Coastal frontogenesis responds to differential warming and moistening in conjunction with sensible heating over the ocean and the blocking of shallow cold air by the southern Appalachian Mountains. The observed wind field is frontogenetical during coastal frontogenesis whereas the large-scale geostrophic flow contributes to frontolysis.

A comparison of kinematic, quasi-geostrophic and semigeostrophic vertical motions reveals that the kinematic method best captures the structure in the lower troposphere, indicative of the importance of boundary layer convergence. The semigeostrophic vertical motions are superior to the quasi-geostrophic vertical motions in depicting a sloping updraft and a closer separation of the ascent–descent dipole. Solution of the semigeostrophic vertical circulation equation from Hoskins and Draghici lends some support to the finding of Uccellini and others that the flow around the subtropical jet streak was unbalanced.

Finally, kinetic energy export from the storm environment is balanced by a positive residual and generation by both the divergent and nondivergent components of the wind in a manner suggestive of an anticyclone region.

1. Introduction

Bosart (1981) described the meteorology of the memorable Presidents' Day snowstorm of 18–19 February 1979 in the Middle Atlantic States. Evidence was presented, based on the analysis of surface observations, which suggested that the incipient cyclone was a shallow, baroclinic boundary layer disturbance that formed along a Carolina coastal front. Differential heating, moistening and roughness between land and sea in conjunction with cold air damning to the east of the Appalachian Mountains were implicated as important physical mechanisms that sustained the incipient cyclogenesis and allowed significant precipitation to develop along the coastal plain. The shallow cyclone then tracked north-northeastward parallel to the coast. Rapid deepening ensued when this cyclone came under the favorable southwesterly flow ahead of a prominent upper tropospheric trough moving eastward from the Ohio Valley. Convection occurred in the vicinity, and to the north, of the rapidly intensifying storm. Whether this convection (e.g., see Sanders and Gyakum, 1980; Gyakum, 1983a,b) had a direct bearing on the storm deepening rate has not been ascertained and will not be discussed here.

Uccellini *et al.* (1984) have shown that prior to rapid cyclogenesis, the upper troposphere was characterized by an amplifying, unbalanced subtropical jet streak. They hypothesized that the thermally indirect circulation associated with the propagating jet streak resulted in a more favorable environment for coastal cyclogenesis through enhanced divergence aloft. In their view, the lower level ageostrophic flow was embedded in the indirect circulation associated with the subtropical jet and influenced by boundary layer and diabatic processes.

The purpose of this paper is to extend and quantify the earlier work of Bosart (1981). Boundary layer processes relevant to coastal frontogenesis and cyclogenesis will be emphasized. The cyclone spinup process is investigated through a kinetic energy, vorticity, potential vorticity and vertical motion diagnosis.

2. Synoptic overview and vertical motion analysis

Objective analyses of temperature, height and winds are presented for the surface, 700 and 300 mb levels

for the 24 h period ending 1200 GMT 19 February 1979 shown in Fig. 1. The analyses were generated on a 1° latitude–longitude mesh every 100 mb from the surface to 100 mb using modified procedures discussed by DiMego and Bosart (1982a) and Boyle and Bosart (1983). The first-guess fields were interpolated from the operational National Meteorological Center (NMC) analyses of height, temperature, relative humidity and wind components given on a 2.5° latitude–longitude mesh. The interpolated observed winds are plotted every 2° of latitude and longitude in Fig. 1 for clarity. (More detail is shown in Figs. 1–3 of Bosart, 1981.)

The development of the strong sea level pressure ridge along the Atlantic coast occurs beneath prominent 700 mb cold advection in a confluent north-

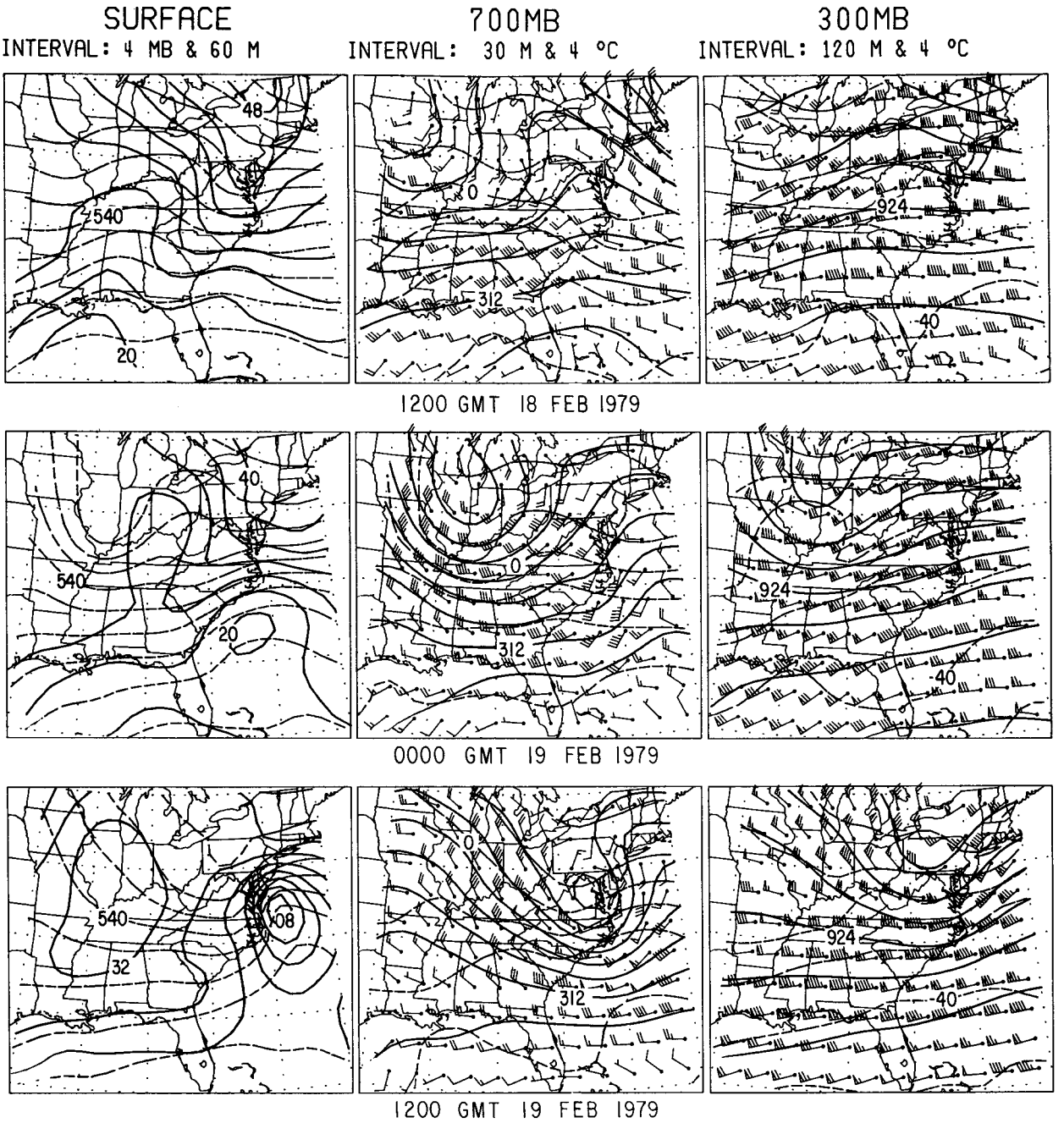

FIG. 1. Surface pressure (mb, solid lines) and 1000–500 mb thickness (dam, dashed lines); 700 and 300 mb objectively analyzed height (dam, solid lines), temperature (°C, dashed lines) and wind for 1200 GMT 18 February 1979 through 1200 GMT 19 February 1979. Each pennant, full barb and half barb denotes 25, 5 and 2.5 m s^{-1}, respectively.

westerly flow that extends upward to 500 mb prior to 1200 GMT 18 February. By 1200 GMT 18 February the confluence and cold advection zone is retreating seaward and a major cold air blocking event east of the Appalachian Mountains is well underway. The outbreak of heavy precipitation to the east of the southern Appalachians by 1200 GMT 18 February occurs with lower tropospheric warm advection to the east of the 300 mb ridge line. Coastal frontogenesis begins at this time and a distinct closed cyclonic circulation along the front is evident 12 h later. Rapid intensification of the shallow coastal cyclone commences around 0600 GMT 19 February (see Bosart, 1981) as the prominent upper tropospheric short wave trough approaches the coast.

Diagnosed kinematic vertical motions are shown in Fig. 2 at 900 and 500 mb for the 24 h period ending 1200 GMT 19 February 1979. The computations were made subject to the boundary condition of zero vertical motion at 1000 and 100 mb and a constant correction to the divergence using the procedure of O'Brien (1970) and Pedder (1981).

For comparison purposes, quasi- and semigeostrophic vertical motions were computed. The quasi-

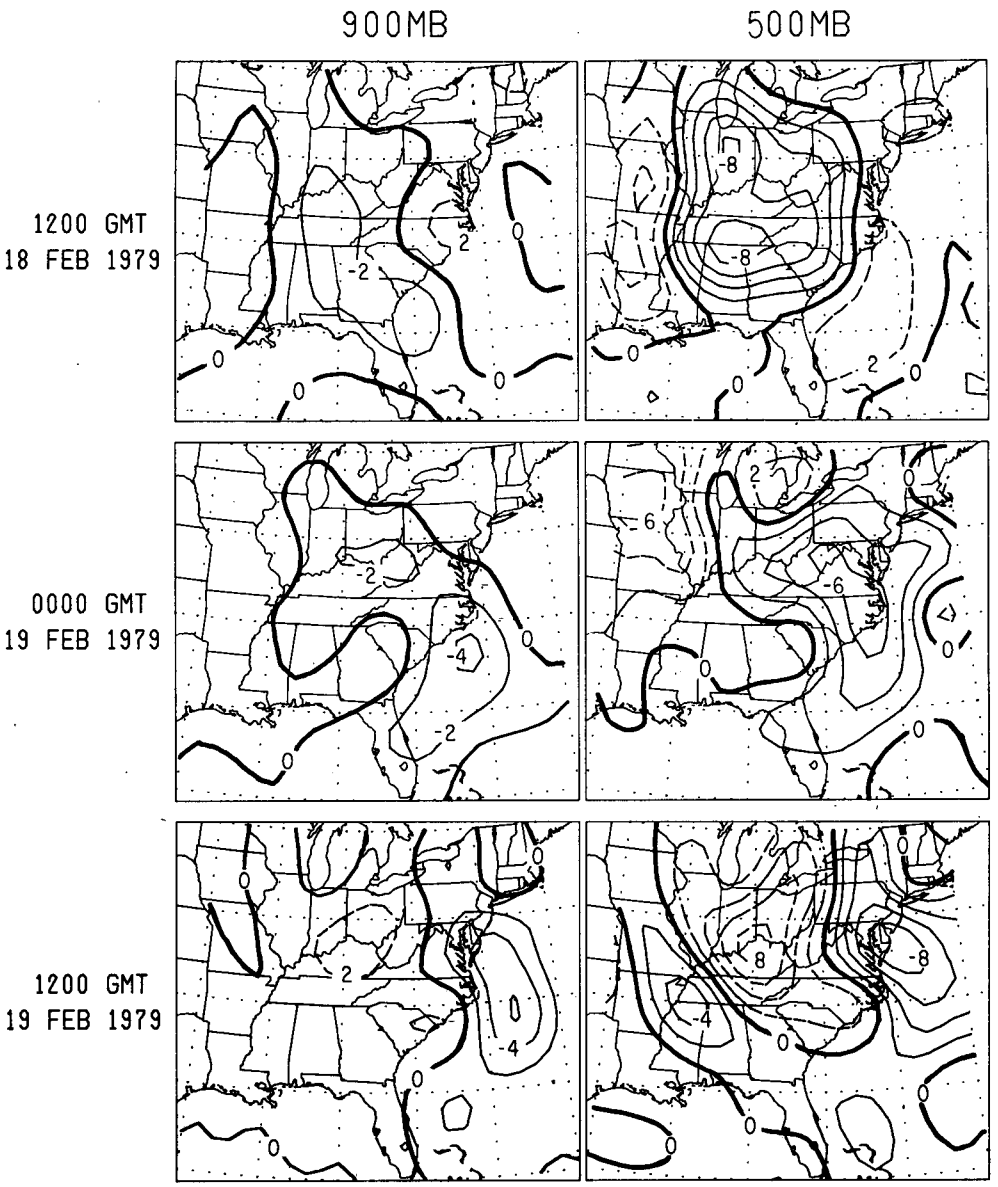

FIG. 2. 900 and 500 mb kinematic vertical motions for 1200 GMT 18 February 1979 through 1200 GMT 19 February 1979. Zero vertical motion, ascent and descent are indicated by heavy solid, thin solid and thin dashed lines, respectively. Contour interval: 2×10^{-3} mb s^{-1}.

geostrophic vertical motions were obtained from Hoskins *et al.* (1978) and Hoskins and Pedder (1980) as follows:

$$\sigma\nabla^2\omega + f^2\frac{\partial^2\omega}{\partial p^2} = -2\nabla\cdot\mathbf{Q}_g, \tag{1}$$

where

$$\sigma = -h\frac{\partial\theta}{\partial p},$$

$$h = \left(\frac{R}{p}\right)\left(\frac{p}{p_0}\right)^{\kappa},$$

$$\mathbf{Q}_g = \left\{f\left(\frac{\partial u_g}{\partial x}\frac{\partial v_g}{\partial p} - \frac{\partial v_g}{\partial x}\frac{\partial u_g}{\partial p}\right),\ f\left(\frac{\partial u_g}{\partial y}\frac{\partial v_g}{\partial p} - \frac{\partial v_g}{\partial y}\frac{\partial u_g}{\partial p}\right)\right\}$$

$$= \left(-h\frac{\partial\mathbf{V}_g}{\partial x}\cdot\nabla\theta,\ -h\frac{\partial\mathbf{V}_g}{\partial y}\cdot\nabla\theta\right).$$

(All symbols in this and the following equations are defined in the Appendix.) Here σ is a measure of the static stability and is taken as a function of pressure only. Use of the thermal wind equation reveals that $\mathbf{Q}_g$ is equal to the rate of change of potential temperature gradient moving with the horizontal geostrophic velocity [$\mathbf{Q}_g = h(d/dt)(\nabla\theta)$] from which it follows that $\mathbf{Q}_g\cdot\nabla\theta$ is a measure of geostrophic frontogenesis. A second-order centered differencing scheme was applied to the grid-point data to calculate the forcing function in (1).

Hoskins and Draghici (1977) derived the semigeostrophic version of (1) as follows:

$$\nabla_x^2(q_g w^*) + f^2\frac{\partial^2 w^*}{\partial Z} = 2\nabla_x\cdot\mathbf{Q}_s, \tag{2}$$

where

$$q_g = \left(\frac{g}{\theta_0}\right)J\frac{\partial\theta}{\partial Z}, \quad \text{(potential vorticity)},$$

$$w^* = w/J,$$

$$\mathbf{Q}_s = \left(-\frac{g}{\theta_0}\frac{\partial\mathbf{V}_g}{\partial X}\cdot\nabla_x\theta,\ -\frac{g}{\theta_0}\frac{\partial\mathbf{V}_g}{\partial Y}\cdot\nabla_x\theta\right),$$

$J = (\zeta_g + f)/f$ (Jacobian of the transformation),

$$X = x + \frac{v_g}{f}, \quad Y = y - \frac{u_g}{f}, \quad Z = z.$$

The interpretation of (2) is analogous to (1), provided that we remember i) X and Y, our new horizontal coordinates, are stretched in physical space with increased (decreased) resolution in regions of cyclonic (anticyclonic) relative vorticity and ii) the effective static stability is no longer a function of z only but is measured by the potential vorticity q_g, a quantity which is advected with the fluid.

Equation (2) was solved analogous to (1) in semigeostrophic coordinates. The gridded input data was interpolated to semigeostrophic space, the calculations were made and the results interpolated back to physical space for display purposes. A smoother was applied to the displayed vertical motion fields. Figures 3a, b depict the quasi-geostrophic and semigeostrophic vertical motion fields and Q-vectors analogous to Fig. 2 at 1200 GMT 18 and 19 February. All vertical motion fields were derived from the objective analyses presented in Fig. 1.

Comparison of Figs. 2 and 3 is interesting. At 1200 GMT 18 February weak quasi-geostrophic and semigeostrophic ascent is found along the southeastern coast of the United States (ascent at 900 mb east of North Carolina at this time appears to be an artifact of the analysis), despite the presence of a significant coastal front and widespread precipitation (see Fig. 4 of Bosart, 1981). At 500 mb all three methods capture the ascent maximum in the lower Great Lakes, although the kinematic ascent maximum is farther east. Neither the quasi-geostrophic nor the semigeostrophic method captures the separate 500 mb ascent maximum over Tennessee. This failure may be a reflection of the unbalanced nature of the flow in the subtropical jet streak as shown by Uccellini *et al.* (1984); their Fig. 16a shows strong midtropospheric ascent in the Tennessee Valley at this time as well.

The kinematic ascent maximizes at 700 mb (not shown) near the coast whereas the quasi-geostrophic and semigeostrophic ascent is a maximum at 500 mb. As noted by Bosart (1981) and Uccellini *et al.* (1984) the prominent lower tropospheric convergence in the wind field across the southeastern United States is considerably reduced in the corresponding geopotential height field. We observe, however, that 900 mb quasi-geostrophic and semigeostrophic frontogenesis ($\mathbf{Q}_g\cdot\nabla\theta$ and $\mathbf{Q}_s\cdot\nabla_x\theta$) is a maximum between the southern Appalachians and the coast and encompasses the region of cold air damming.

By 0000 GMT 19 February the kinematic ascent lies along the North Carolina coast with a maximum in excess of -10×10^{-3} mb s^{-1} at 700 mb. The approaching Ohio Valley trough is best defined at 500 and 300 mb (not shown). The quasi-geostrophic and semigeostrophic vertical motions (not shown) are now in better agreement with the kinematic vertical motion near the coast although the intensity remains underestimated. With the onset of explosive cyclonic deepening by 1200 GMT 19 February, the quasi-geostrophic and semigeostrophic ascent–descent couplet becomes very well defined with the maximum computed ascent approaching -30×10^{-3} mb s^{-1} between 700 and 500 mb. This will support a surface precipitation rate of 7.5 mm h^{-1} with the assumption of a parobolic vertical motion profile in a saturated atmosphere and neglecting evaporation. Comparison with the observed precipitation totals suggests these values are too large by a factor of 2, although individual air parcels may encounter such ascent briefly. The broad kinematic ascent of -10×10^{-3}

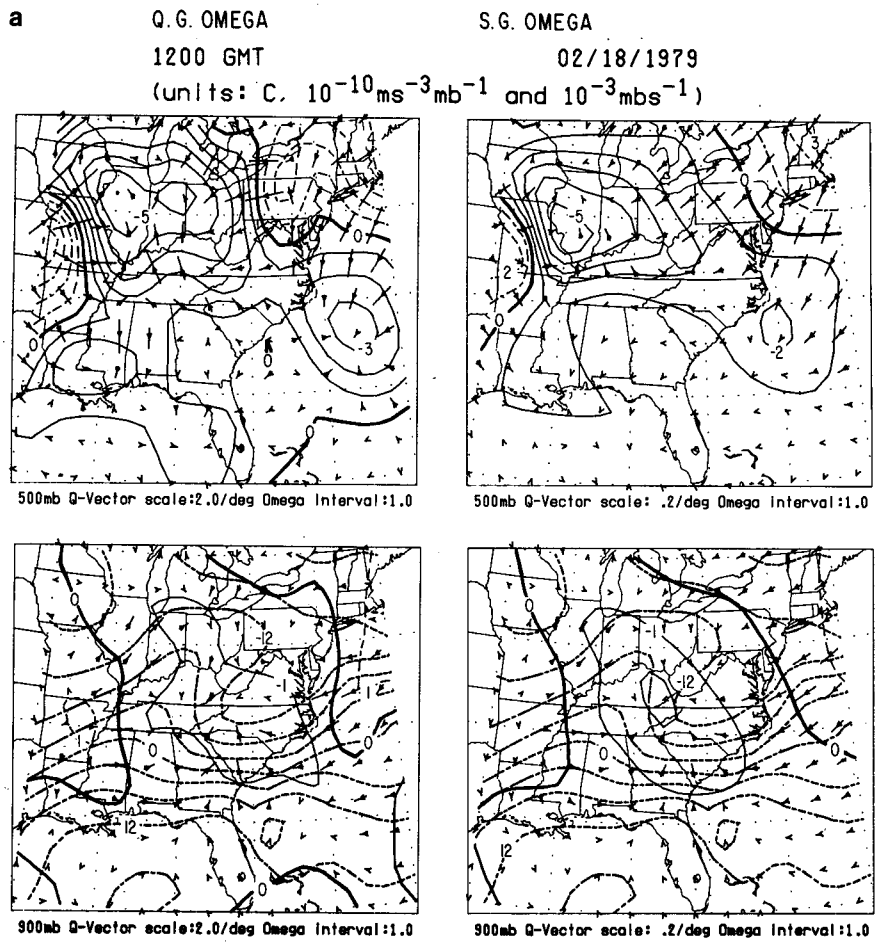

FIG. 3. 900 mb temperature (short dashed lines with 4°C interval); 900 mb and 500 mb quasi-geostrophic and semigeostrophic **Q**-vectors (10^{-10} m s^{-3} mb^{-1} and 10^{-10} s^{-3}) and vertical motions (10^{-3} mb s^{-1}, contour interval as indicated) for 1200 GMT 18 (a) and 19 (b) February 1979. Zero vertical motion, ascent and descent are indicated by heavy solid, thin solid and long thin dashed lines, respectively.

mb s^{-1} between 700 and 500 mb suggests a grid volume average precipitation rate of 2.5 mm h^{-1}, which is more in keeping with observation.

A comparison of the quasi-geostrophic and semigeostrophic vertical motions at the onset of explosive cyclogenesis is insightful. The semigeostrophic couplet is both more intense and more closely spaced compared to the quasi-geostrophic couplet. The maximum semigeostrophic ascent in the 700–500 mb layer lies over Chesapeake Bay, very close to the surface and radar-derived precipitation maximum, whereas the quasi-geostrophic ascent maximizes just offshore. Warm frontogenesis is confined to the region immediately ahead of the cyclone at 900 mb in both methods. The absence of any indicated appreciable southward cold air push in the wake of the cyclone is supported by observation. Another interesting feature is that the semigeostrophic ascent–descent dipole shows a significant northward tilt with decreasing pressure. This is more physically realistic than the nearly vertical quasi-geostrophic couplet and supports the idea of a sloping conveyer belt-relative flow (e.g., see Carlson, 1980), in agreement with the kinematic results. We note with interest, however, that valuable forecast information is contained in the semigeostrophic vertical motion fields with regard to the maximum precipitation region and the timing of the abrupt cessation of precipitation.

In this particular case, given the immense advantage of hindsight, the kinematic vertical motions are superior in alerting forecasters to coastal redevelopment. A similar conclusion, also on the basis of a single case study, was reached by Smith and Lin (1978). We speculate that the apparent superiority of the kinematic method is a reflection of the importance of the lower tropospheric ageostrophic wind field (see Fig. 4) in producing a swath of convergence (below 700 mb) along the coast by 1200 GMT 18 February.

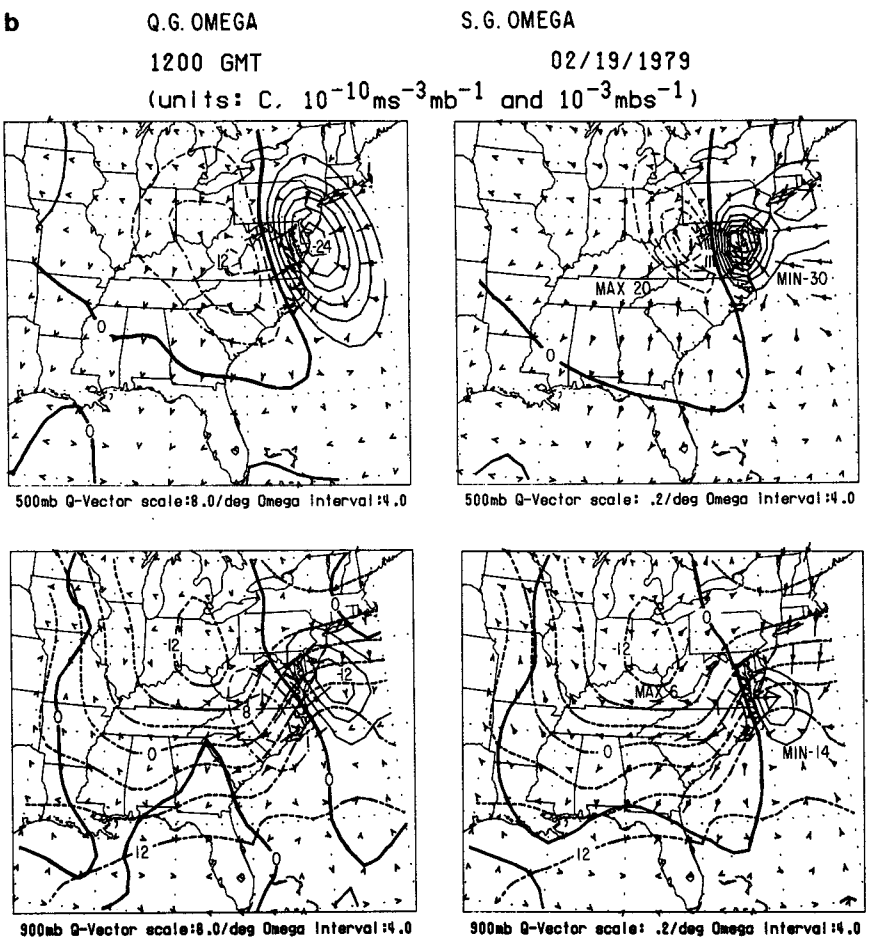

FIG. 3. (*Continued*)

It will be especially important to initialize mesoscale prediction models with a wind field of sufficient vertical and horizontal resolution to predict cyclones of this type successfully, a point previously suggested by Bosart (1981).

All vertical motion methods reveal the consolidation of the ascent center between 0000 and 1200 GMT 19 February along the Middle Atlantic coast as explosive cyclogenesis begins. An interesting question to consider is the timing of the cyclogenesis. The shallow, cyclonic circulation associated with the coastal front drifted north-northeastward (see also Bosart, 1981) parallel to the coastline and into a more favorable position for deepening ahead of the eastward moving short wave in the Ohio Valley. The absence of appreciable cyclogenesis (in terms of closed isobars around a cyclone) west of the Appalachians, despite the passage of a strong short wave aloft, may be related to the presence of a very stable boundary with a quasi-uniform potential temperature structure in that region. Recall that the lower tropospheric baroclinicity is highly concentrated between the Appalachians and the coast.

The ageostrophic wind field, derived by subtracting the computed geostrophic wind from the observed wind in Fig. 1, is shown in Fig. 4 together with the height field. At 900 mb the northeasterly, ageostrophic wind maximizes in the Carolinas at 1200 GMT 18 February (coincident with the onset of coastal frontogenesis) with the maximum convergence in eastern Georgia. A similar pattern is seen at 700 mb with the winds rotated clockwise by 120° indicative of the strong warm advection occurring in this region. At 300 mb a pattern consistent with supergeostrophic (subgeostrophic) flow in a ridge (trough) is seen throughout. An interesting exception occurs at 1200 GMT 18 February (also at 0000 GMT 19 February across New England) when cross contour flow toward lower heights is seen well to the east of the 300 mb ridge line. This agrees with Uccellini *et al.* (1984) who have shown the vertical coupling of the ageostrophic circulations.

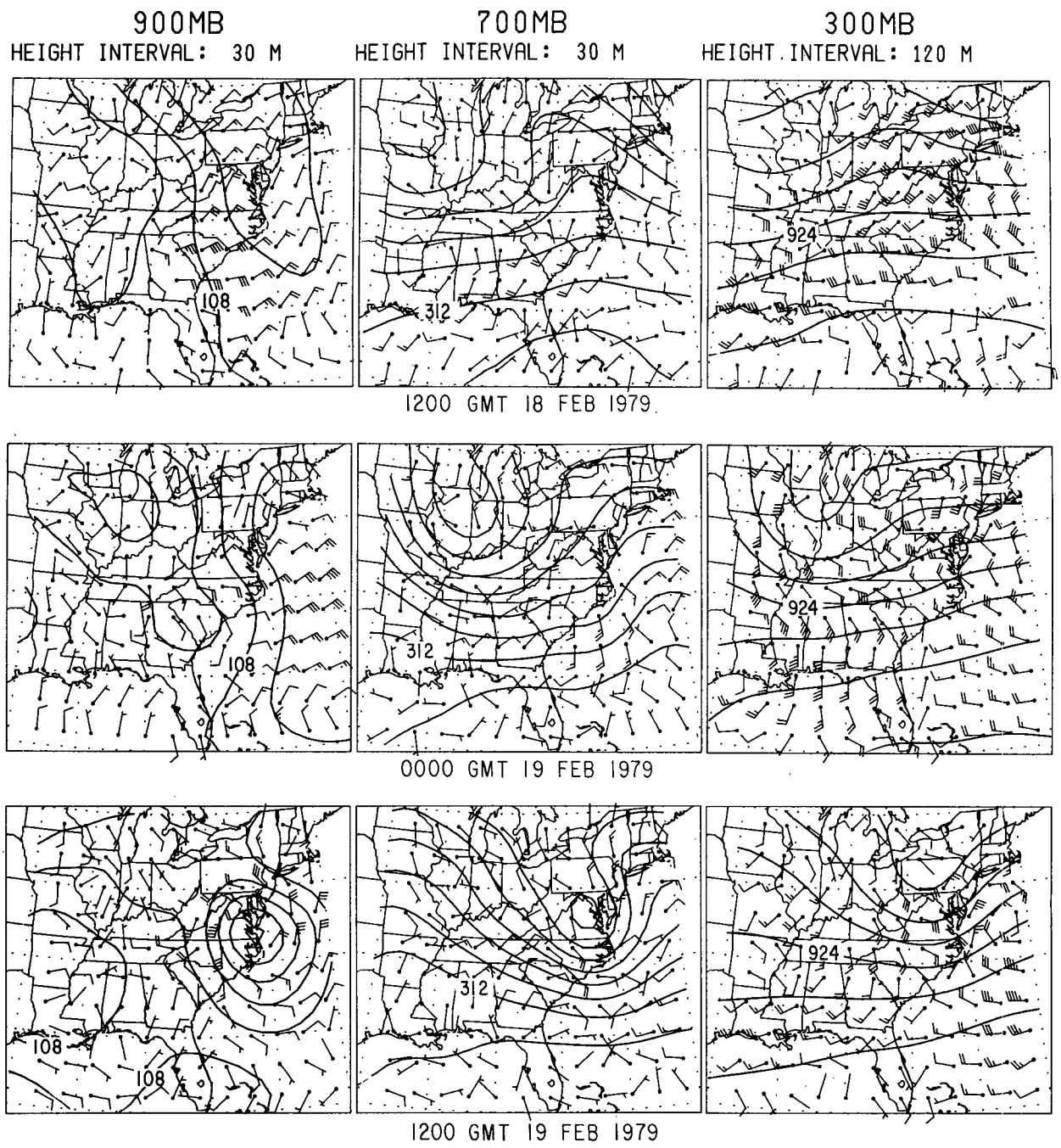

FIG. 4. Geopotential height (dam, solid lines) and ageostrophic wind at 900, 700 and 300 mb for 1200 GMT 18 February 1979 through 1200 GMT 19 February 1979. Each pennant, full barb and half barb denotes 25, 5 and 2.5 m s^{-1}, respectively.

3. Moisture budget

The difference between precipitation (P) and evaporation (E) can be expressed as

$$P - E = -\frac{1}{g}\int_{p_t}^{p_b}\left(\frac{\partial q}{\partial t} + \nabla\cdot q\mathbf{V} + \frac{\partial q\omega}{\partial p}\right)dp, \quad (3)$$

where q represents the specific humidity. The subscripts b and t refer to the pressure at the base and top of the level, respectively. The terms on the right-hand side of (3) represent the change in storage and horizontal and vertical flux divergence.

A map of $-\nabla\cdot q\mathbf{V}$ for the surface to 700 mb layer over the 36 h period ending 1200 GMT 19 February

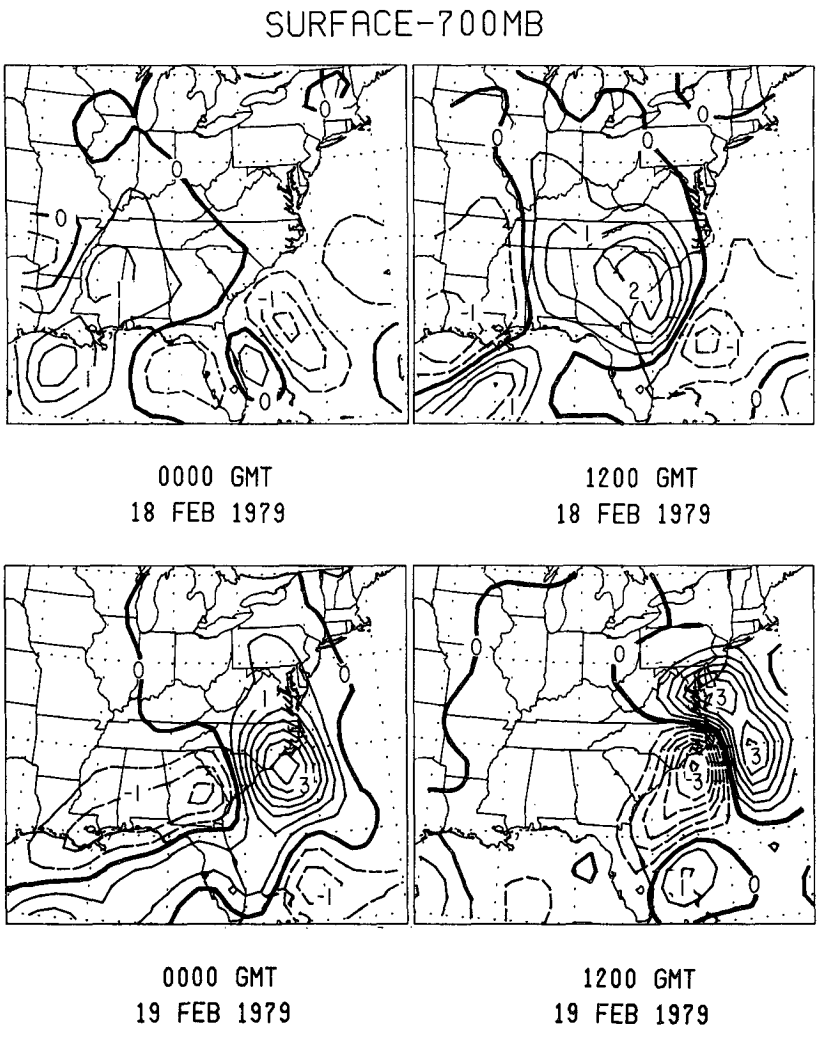

FIG. 5. Surface–700 mb layer moisture flux convergence ($-\nabla \cdot qV$) at the indicated times. Zero contour, convergence and divergence are indicated by heavy solid, thin solid and thin dashed lines, respectively. Contour interval: 0.5 mm h^{-1}.

appears in Fig. 5. At 0000 GMT 18 February moisture flux convergence is concentrated west of the Appalachian Mountains. With the onset of coastal frontogenesis 12 h later, the moisture flux convergence expands eastward and intensifies. Subsequent to 1200 GMT 18 February the coastal maximum intensifies while moving slowly northward. The cyclonic rotation of the convergence–divergence dipole as cyclogenesis develops is evident.

A breakdown of the moisture divergence term into its advective and divergent components was also carried out for the regions shown in Fig. 6. Area 1 represents the location of the initial upper tropospheric vortex while sector 2 includes the domain of the cold anticyclone and later rapid cyclogenesis. Region 3, west of the Appalachians, features little activity, while

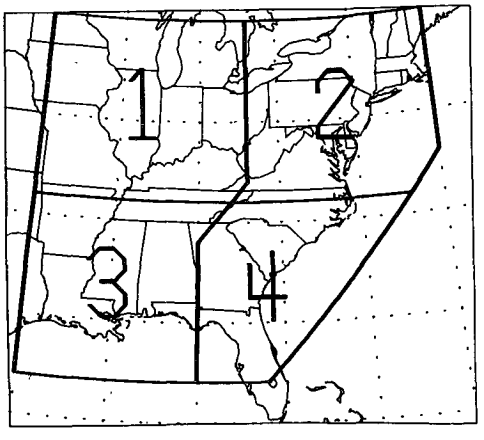

FIG. 6. Map of partitional areas for selected computations.

sector 4 includes the region of coastal frontogenesis and incipient cyclogenesis. The contribution to advection by the rotational and divergent part of the wind together with the divergence term is given in Fig. 7 for areas 2 and 4. The numbers represent averages computed over the grid points in each region.

A number of important differences are seen in Fig. 7. Region 2 finds nearly equal contributions from $-q\nabla\cdot\mathbf{V}_D$ and $-\mathbf{V}_R\cdot\nabla q$ below 600 mb, opposed by $-\mathbf{V}_D\cdot\nabla q$, beginning 0000 GMT 19 February. Region 4 illustrates the dominant role of moisture flux convergence (primarily due to $-q\nabla\cdot\mathbf{V}_D$) in the boundary layer in providing water vapor for precipitation growth accompanying coastal frontogenesis for the 12 h period ending 0000 GMT 19 February. An important difference, however, is that convergence dominates advection throughout in region 4, suggesting the importance of ageostrophic motions in the boundary layer in providing *in situ* moisture for precipitation development. Farther north in region 2 advective processes are more important initially in moistening the atmosphere, with convergence becoming slightly dominant during the time of rapid cyclogenesis.

4. Vorticity structure

The Eulerian vorticity equation can be written as

$$\frac{\partial\zeta}{\partial t} = -\mathbf{V}\cdot\nabla(\zeta+f) - \omega\frac{\partial\zeta}{\partial p} - (\zeta+f)\nabla\cdot\mathbf{V} - \mathbf{k}\cdot\nabla\omega\times\frac{\partial\mathbf{V}}{\partial p}, \quad (4)$$

where ζ is the relative vorticity. The terms on the right-hand side of (4) are the horizontal and vertical advection of absolute vorticity, vorticity production by convergence and the twisting term.

Figures 8 and 9 depict the advection of absolute vorticity and vorticity production by convergence for

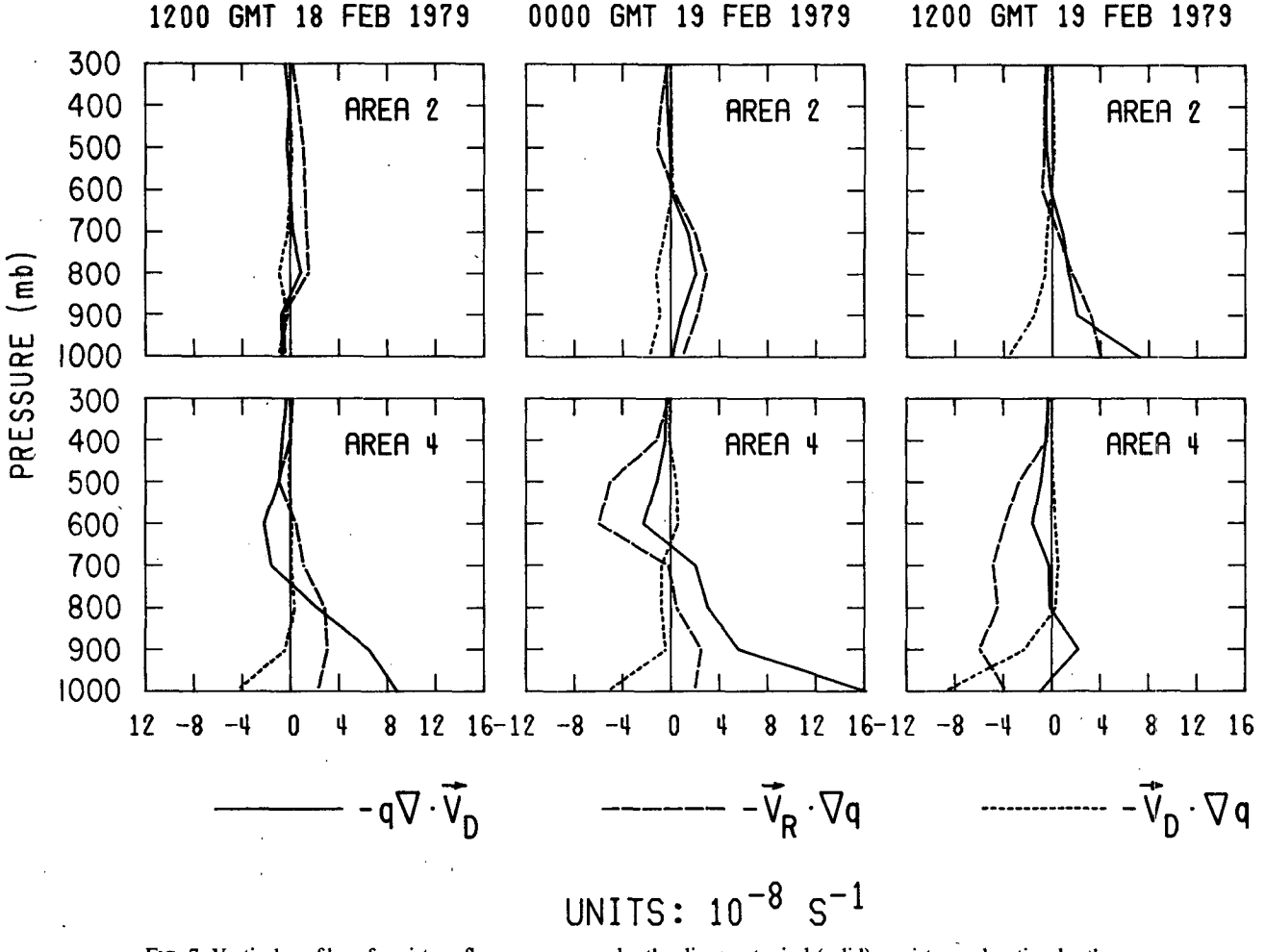

FIG. 7. Vertical profiles of moisture flux convergence by the divergent wind (solid); moisture advection by the nondivergent (long dashed) and divergent (short dashed) wind for areas 2 and 4 defined in Fig. 6. Units: 10^{-8} s^{-1}.

selected isobaric levels at 1200 GMT 18 and 19 February 1979. During the time of incipient coastal frontogenesis (Fig. 8) vorticity production along the Carolina coast is restricted to convergence at 900 and 700 mb (not shown). The advection of absolute vorticity contributes to vorticity destruction, particularly in the mid and upper troposphere over northeast Georgia and western South Carolina. The rapid cyclogenetic phase (Fig. 9) features the more typical vorticity production by convergence and advection in the lower and upper troposphere, respectively. These ideas are further summarized in time section format for regions 2 and 4 (cf. Fig. 6) in Fig. 10. (Caution: the vertical scale varies for clarity.)

The vorticity analysis results for the southeastern United States (area 4) reveal that vorticity production by convergence dominates the incipient cyclogenetic environment in the surface to the 700 mb layer at 1200 GMT 18 February and 0000 GMT 19 February. Cyclonic vorticity advection is of lesser importance, except at 0000 GMT 19 February in the 400–100 mb layer. The vertical advection of vorticity (usually neglected in synoptic-scale studies) is of some significance in the 700–400 mb layer in region 4. It and the twisting term are the only sources of vorticity at 1200 GMT 18 February. At 0000 GMT 19 February the vertical advection of vorticity is comparable to the horizontal advection of vorticity in region 4. Vorticity is destroyed by divergence in the 700–400 mb layer throughout. We note that the southeastern United States cross section profile for 1200 GMT 18 February given in Uccellini *et al.* (1984, Fig. 16a) depicts widespread divergence above 700 mb. We speculate that vorticity is produced by convergence below 700 mb in the highly ageostrophic flow. The aforementioned ascent maximum in the lower troposphere helps to advect some of this vorticity upward as the cyclone spins up.

Arnason and Carstensen (1959) showed that the twisting and vertical advection terms in the vorticity equation should have an out-of-phase relationship for synoptic-scale motions. DiMego and Bosart (1982b) showed that this tended to be the case for Tropical Storm Agnes in June 1972. This is not the case in region 4 where the twisting term is of some significance in the 700–400 and 400–100 mb layers at 1200 GMT 18 February. It is possible that the relative importance of the twisting term at this time is a reflection of the vigorous thermally indirect circulation in the presence of the strong subtropical jet streak as documented by Uccellini *et al.* (1984).

Comparison with area 2 (Fig. 10) shows a picture more in keeping with classical cyclogenesis as described by, e.g., Petterssen (1955), and Cressman (1961) and Chen and Bosart (1979). Advective processes begin to dominate after 0000 GMT 19 February in region 2 where rapid cyclogenesis takes place. Vorticity production by convergence now extends upward through the middle troposphere. Comparison with Figs. 8 and 9 reveals that this interpretation is not an artifact of the Eulerian framework.

We conclude that the rapid development stage of the Presidents' Day Storm is analogous to a type B development as described by Petterssen and Smebye (1971), in which surface development responds to the approach of powerful cyclonic vorticity advection aloft. There is one crucial difference, however. In the present case, *in situ* vorticity production by the aforementioned physical mechanisms in the lower troposphere means that the atmosphere is very ripe for a rapid spinup with the approach of the upper level trough because the rate of generation of vorticity by convergence is directly proportional to the intensity of the existing lower tropospheric cyclonic circulation. A similar phenomenon was observed for Tropical Storm Agnes by DiMego and Bosart (1982b).

5. Potential vorticity structure

According to Hoskins and Draghici (1977), conservation of potential vorticity in semigeostrophic space yields

$$\left(D_g + w\frac{\partial}{\partial z}\right)q_g = 0, \tag{5}$$

where

$$\left.\begin{aligned} D_g &= \frac{\partial}{\partial T} + u_g\frac{\partial}{\partial X} + v_g\frac{\partial}{\partial Y} \\ T &= t \end{aligned}\right\}.$$

Cross sections of semigeostrophic potential vorticity along selected longitudes and latitudes are displayed in Fig. 11 over the background potential temperature field. (North–south cross sections are taken along the coastal front; east–west cross sections are taken through the migratory short wave trough.) Centered differences were used to compute q_g in semigeostrophic space, and the results were interpolated back to physical space for display purposes.

At 1200 GMT 18 February coastal frontogenesis south of 35°N (80°W) occurs in a weak semigeostrophic potential vorticity environment. Slightly larger values to the north coincide with a warm advection region (Fig. 1). In contrast, the semigeostrophic potential vorticity is high above 300 mb between 90 and 95°W, as the cold short wave trough advances eastward (note that contour interval is halved). A weaker, secondary maximum is found below 800 mb, extending eastward to the Appalachian highlands. By 0000 GMT 19 February the strengthening coastal front circulation is coincident with a weak boundary layer potential vorticity maximum along 80°W. The corresponding 39°N latitudinal

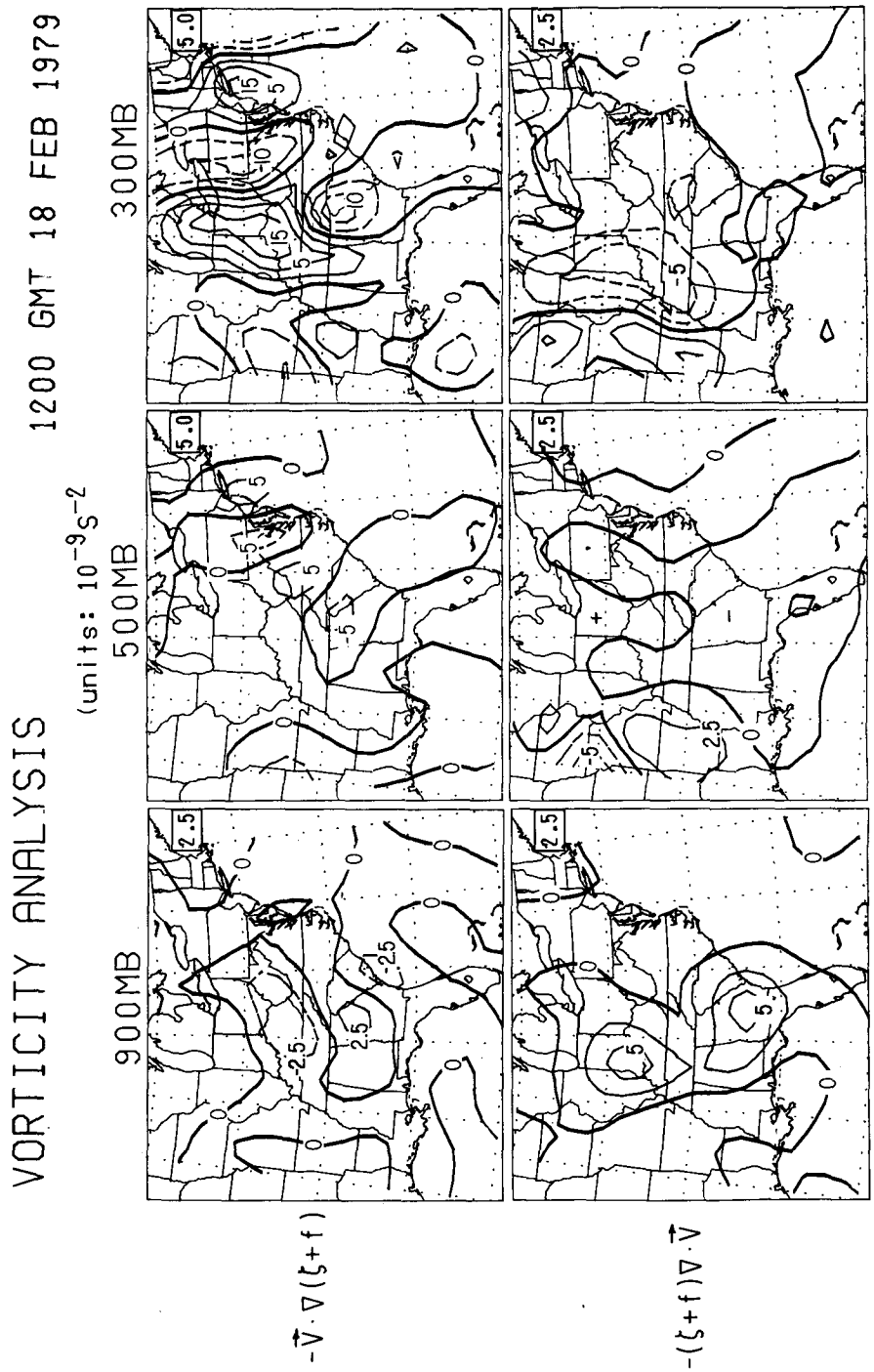

FIG. 8. Advection of absolute vorticity (top panels) and vorticity production by convergence (bottom panels) at 900, 500 and 300 mb for 1200 GMT 18 February 1979. Zero contour heavy solid with positive (negative) values given by thin solid (dashed) lines. Contour interval in small box in upper right corner of each panel. Units: 10^{-9} s^{-2}.

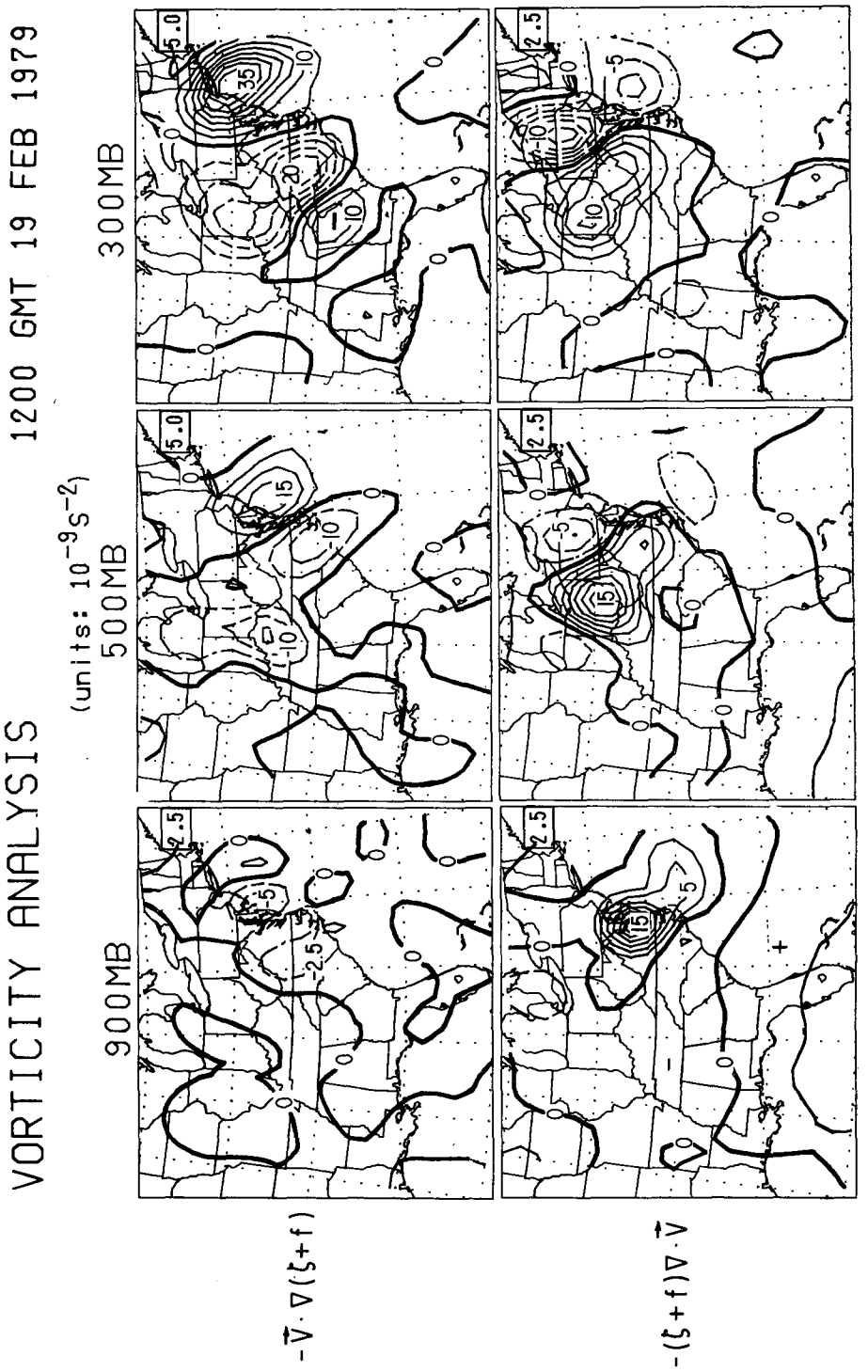

FIG. 9. As in Fig. 8 except for 1200 GMT 19 February 1979.

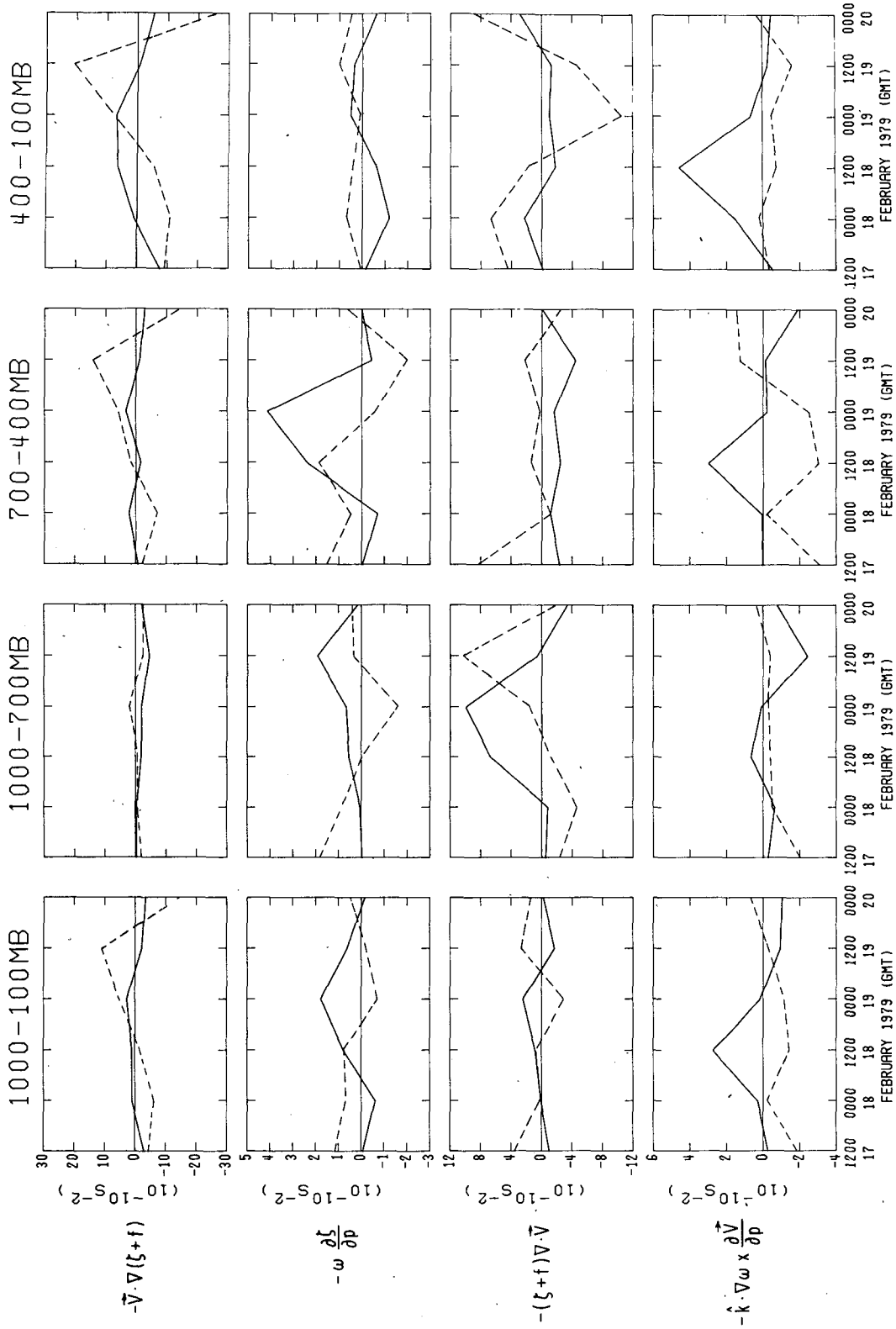

FIG. 10. Vorticity time series analysis for indicated layers in areas 2 (dashed) and 4 (solid) as defined in Fig. 6. Note variation in vertical scale.

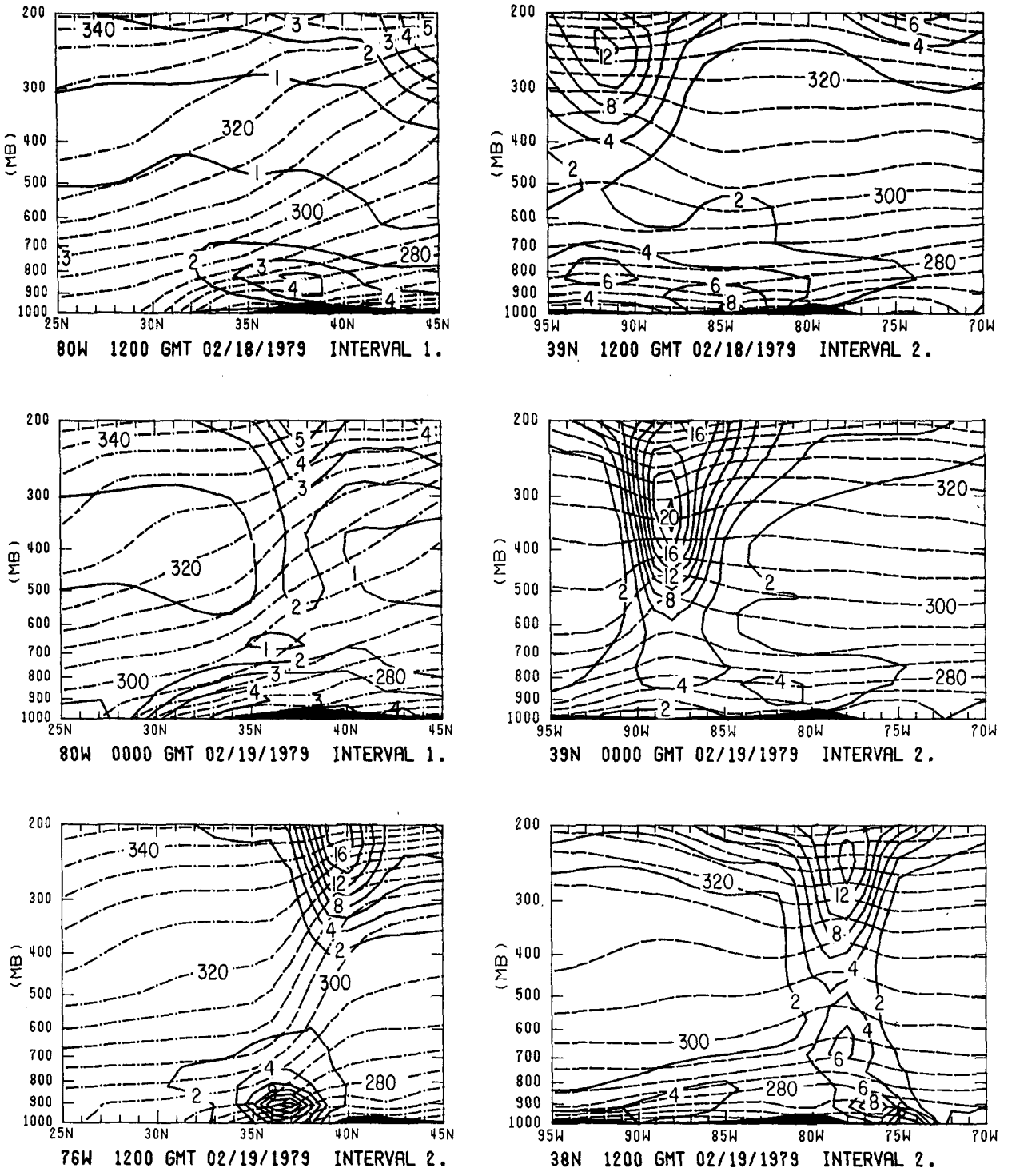

FIG. 11. Cross sections of semigeostrophic potential vorticity (10^{-4} s^{-2}, solid) and potential temperature (every 5 K, dashed) along selected longitudes and latitudes for 1200 GMT 18 February through 1200 GMT 19 February 1979. The potential vorticity contour interval is indicated below lower right corner of each panel.

cross section depicts the eastward propagation, intensification and downward extension of the potential vorticity maximum (independent of the cross section latitude—not shown). The east–west potential temperature gradient remains weak beneath this maximum.

By 1200 GMT 19 February substantial growth in semigeostrophic potential vorticity below 800 mb is seen. The longitudinal section along 76°W suggests distinct lower and upper tropospheric maxima with the former located about 150 km west of the rapidly deepening surface cyclone center. A similar cross section along 78°W (not shown) indicates that both maxima are connected, a picture consistent with the latitudinal cross section along 38°N. [The upper (lower) tropospheric maximum dominates along 39°N (37°N)—not shown.] The growth of lower tropospheric semigeostrophic potential vorticity accompanies the steepening of the north–south gradient of potential temperature between 300 and 700 mb and the tightening of the boundary layer potential temperature gradient.

Overall, the relatively high value of semigeostrophic potential vorticity associated with the Ohio Valley trough moves eastward and is located northwest of the surface cyclone at the time of onset of rapid cyclogenesis. A tongue of higher potential vorticity air extends downward to the south and east with a secondary maximum in the boundary layer on the cold side of the coastal front. It appears that boundary layer semigeostrophic potential vorticity growth occurs *in situ* with coastal frontogenesis, with a pronounced maximum already evident at the *onset* of rapid surface deepening at 1200 GMT 19 February.

Uccellini *et al.* (1984, 1985) first demonstrated that a tropopause fold occurred upstream 12–24 h *prior* to rapid cyclogenesis. The fold formed near the axis of the strengthening polar front jet in the central United States. High potential vorticity air from the lower stratosphere subsided to near 800 mb to the west of the cyclone in the 12 h prior to rapid development. Uccellini *et al.* (1985) found that potential vorticity was not strictly conserved and that there was some evidence for the existence of a separate maximum of potential vorticity below 800 mb in the Carolinas by 0000 GMT 19 February which also influenced the cyclogenetic region. A similar finding is indicated for the semigeostrophic potential vorticity analysis in Fig. 11. The 12 h time period between observations is too coarse to resolve the interesting time evolution of potential vorticity structure. However, we speculate that the diabatic generation and destruction of potential vorticity is apt to be important in this case.

The position of the potential vorticity maximum on the cold side of the baroclinic zone with respect to the surface front and cyclone is in agreement with Bleck (1973, 1974) and Boyle and Bosart (1983). This is a reflection of the large gradient of potential temperature oriented normal to the coast in the boundary layer. This suggests that an Ertel potential vorticity analysis will yield the maximum potential for vortex tube stretching (and cyclogenesis) as the upper level potential vorticity maximum approaches the coastal baroclinic zone east of the mountains, consistent with the delay in explosive cyclogenesis until 1200 GMT 19 February.

We hypothesize that the production of cyclonic vorticity along the coast by convergence in the lower troposphere in the incipient cyclogenesis stage is vital to the eventual rapid storm spinup phase. The zone of enhanced lower tropospheric vorticity is gradually displaced northeastward, parallel to the coast as coastal frontogenesis proceeds. The juxtaposition of this zone with the region of powerful cyclonic vorticity advection aloft by 1200 GMT 19 February sets the stage for rapid cyclone spinup as lower tropospheric convergence beneath the vigorous short wave acts upon air parcels that have previously acquired considerable cyclonic vorticity. The air mass itself has been warmed and moistened by oceanic sensible and latent heat fluxes with a consequent reduction in the static stability.

Convection in the storm spinup region was documented by Bosart (1981). An analysis of the Patuxent River, Maryland and Cape Hatteras, North Carolina National Weather Service WSR 57 10 cm radar film imagery (not shown) suggests that convection begins as an enhanced line of north–south oriented echoes across North Carolina and Virginia between 0600 and 0900 GMT 19 February as the coastal front continues to develop northward. Meanwhile, the lower tropospheric static stability remains very high between the coast and the Appalachians in response to cold air damming. The resulting static stability gradient normal to the coastline means that vortex tube stretching will be particularly effective in spinning up a cyclone as the potential vorticity maximum aloft reaches the coast.

We note, however, that this view is entirely consistent with our vorticity analysis whereby high vorticity air in the lower troposphere is advected upward in response to the arrival of a vigorous short wave trough. We then suggest, as a physical hypothesis for testing elsewhere, that cold air damming effectively displaces the "eastern slopes" of the Appalachian mountains toward the coast as far as the free atmosphere above the boundary layer is concerned. This may help to explain, in part, why secondary cyclogenesis along the East Coast of the United States (see, e.g., Pagnotti and Bosart, 1984) occurs farther eastward then would be expected by simple vortex tube stretching arguments as air parcels cross to the lee of the Appalachian Mountains.

6. Kinetic energy structure

The Eulerian kinetic energy equation for a layer of air over a region can be expressed as

$$\frac{1}{gS}\int_p\int_S \frac{\partial k}{\partial t}\,dpdS = -\frac{1}{gS}\int_p\int_S \nabla\cdot(k\mathbf{V})dpdS$$
$$-\frac{1}{gS}\int_p\int_S \frac{\partial k\omega}{\partial p}\,dpdS - \frac{1}{gS}\int_p\int_S \mathbf{V}\cdot\nabla\Phi dpdS + D(k), \quad (6)$$

where $k = \frac{1}{2}\mathbf{V}\cdot\mathbf{V}$ is the kinetic energy per unit mass and S is the area of the computational domain. The terms on the right-hand side of (6) are the horizontal and vertical flux divergence of kinetic energy, the generation of kinetic energy due to cross contour flow and the dissipation of kinetic energy.

Maps of the generation of kinetic energy by cross contour flow ($-\mathbf{V}\cdot\nabla\Phi$) are displayed in Figs. 12 and 13 for the 900, 500 and 300 mb levels at 1200 GMT 18 and 19 February, along with the conversion term from eddy available potential energy to eddy kinetic energy, $-\omega'\alpha'$. At 0000 GMT 18 February (not shown) $-\omega'\alpha'$ is <0 (>0) along the southeast coast and central midwest (lower Mississippi Valley and northeastern United States), suggestive of a thermally indirect (direct) circulation in these regions. The effects are strongest at 500 and 300 mb but can be seen clearly at 700 mb and to some extent at 900 mb. At 500 mb $-\mathbf{V}\cdot\nabla\Phi$ is in phase with $-\omega'\alpha'$, consistent with the idea of a thermally direct and indirect circulation. Otherwise, the field of $-\mathbf{V}\cdot\nabla\Phi$ reveals little, except for a broad region of kinetic energy generation at 300 mb north of 35°N.

By 1200 GMT 18 February (Fig. 12) the previously described pattern has been displaced eastward. A thermally direct circulation is found over the incipient coastal front in the lower troposphere. Kinetic energy generation by cross contour flow toward lower heights is found at most levels and extends east of the ridge line at 300 mb. The reversal in sign of $-\omega'\alpha'$ between 0000 and 1200 GMT 18 February occurs with the onset of the thermally direct coastal front circulation in the lower troposphere and the relaxation of the thermally indirect circulation in the mid and upper troposphere as the ridge line advances eastward.

As cyclogenesis evolves (Fig. 13), the aforementioned thermally direct circulation is confined to the warm, oceanic side of the baroclinic zone. A thermally indirect circulation is found over the heavy snow region of the Middle Atlantic States where cold air is being forced to rise relative to warmer air on the storm periphery (recall the absence of significant cold advection in the wake of the storm). Kinetic energy generation by the divergent component of the wind is dominant at 900 and 700 mb in the storm region and significant at 500 and 300 mb, where it tends to oppose kinetic energy destruction by the nondivergent part of the wind (not shown).

The areal and time-averaged horizontal flux of kinetic energy, generation of kinetic energy and dissipation for the total domain shown in Fig. 6 is -70, $+45$ and $+20$ W m^{-2}, respectively. A net export of kinetic energy is indicated during the life cycle of the Presidents' Day cyclone. This export maximizes in the northeast quadrant during the earlier time periods and in the southern quadrants at the later times. Import is confined to the southeastern region prior to 1200 GMT 18 February as the crest of the subtropical jet stream enters the region.

Of interest is the partitioning of the generation of kinetic energy into divergent and nondivergent components ($-\mathbf{V}_D\cdot\nabla\Phi$ and $-\mathbf{V}_R\cdot\nabla\Phi$) to represent the baroclinic and barotropic components as suggested by Pearce (1974). Overall there are nearly equal contributions to kinetic energy generation by the divergent and nondivergent wind (not shown) in the vertical integral. The so-called barotropic conversion is more important in both regions west of the mountains, whereas the baroclinic conversion tends to dominate east of the mountains, except around 1200 GMT 18 February in the southeast sector. Negative values of the barotropic term east of the mountains imply that the nondivergent wind is tending to blow towards higher pressure. The horizontal maps (not shown) clearly show the importance of baroclinic processes to storm development in the lower and midtroposphere, initially and throughout the troposphere at the explosive cyclogenesis stage. Barotropic processes contribute weakly to the initial development before becoming strongly negative in the upper troposphere at 1200 GMT 19 February.

Comparison with Chen *et al.* (1978) shows that barotropic processes are relatively more important in the Presidents' Day case in generating kinetic energy in the storm environment, whereas baroclinic processes dominate the immediate storm area just prior to and during intensification. The pattern of cross contour nondivergent flow toward higher (lower) height in the northwesterly (southwesterly) flow of a developing baroclinic wave found by Krishnamurti (1968) is reversed at 500 mb and, especially, at 300 mb. The winds, while subgeostrophic in the trough (Figs. 1 and 4), have a definite ageostrophic component toward higher height in advance of the trough line.

The development of the Presidents' Day cyclone bears some similarity to what occurred in a numerical experiment of Alpine lee cyclogenesis as described by Tibaldi *et al.* (1980) in that baroclinic processes become increasingly more important as the time of rapid cyclogenesis approaches.

A positive residual is noted everywhere in the overall integral (not shown), particularly east of the mountains in the 400–100 mb layer. Large, positive residuals dominate the 24 h period ending 0000 GMT 19 February in the northeast sector with the approach and passage of a ridge line from the west. Positive

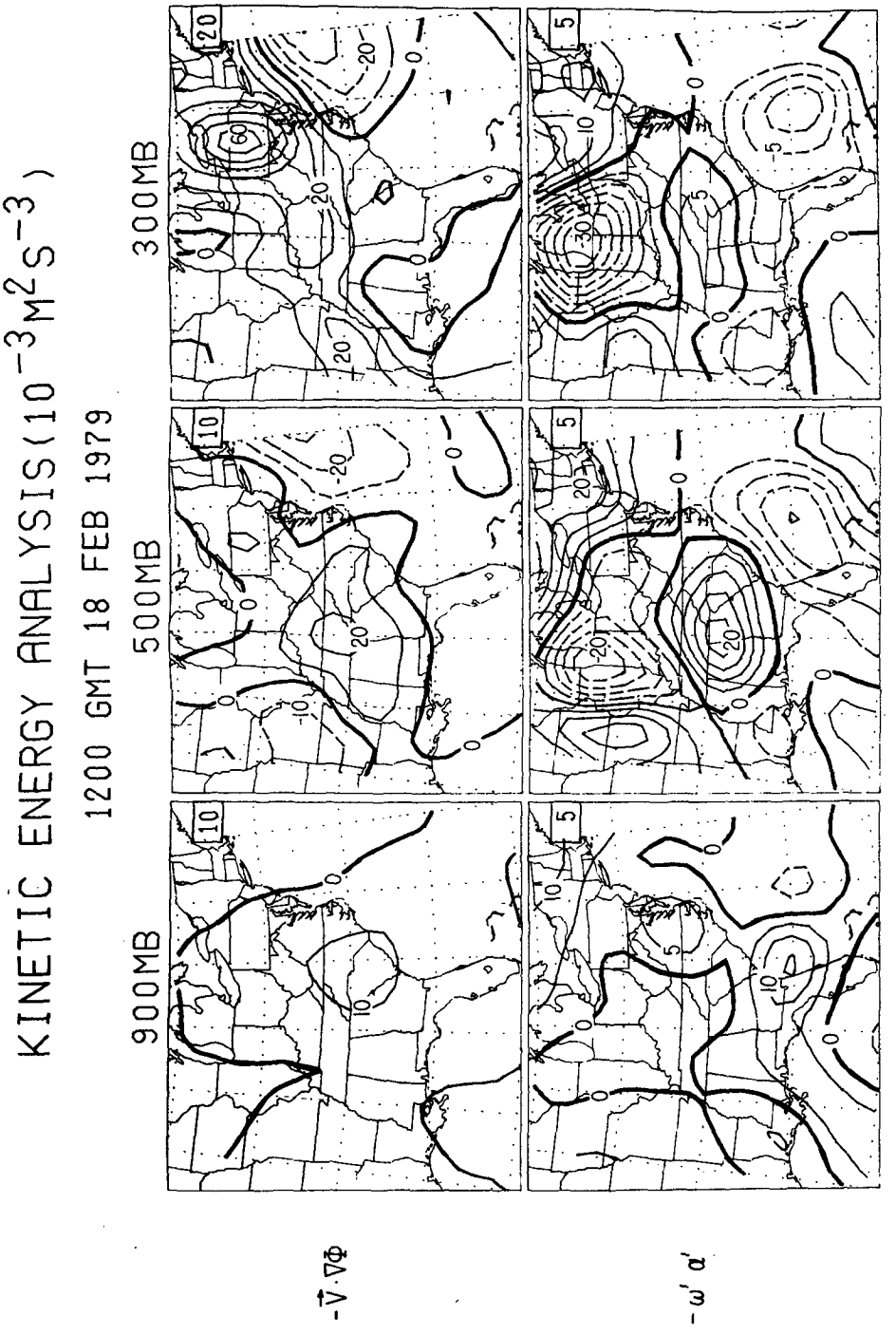

FIG. 12. Generation of kinetic energy (top panels) and conversion term (bottom panels) for 1200 GMT 18 February 1979 at the indicated levels. Zero contour (heavy solid) with generation (destruction) given by thin solid (dashed) contours. Contour interval in small box in upper right corner of each panel. Units: 10^{-3} m^2 s^{-3}.

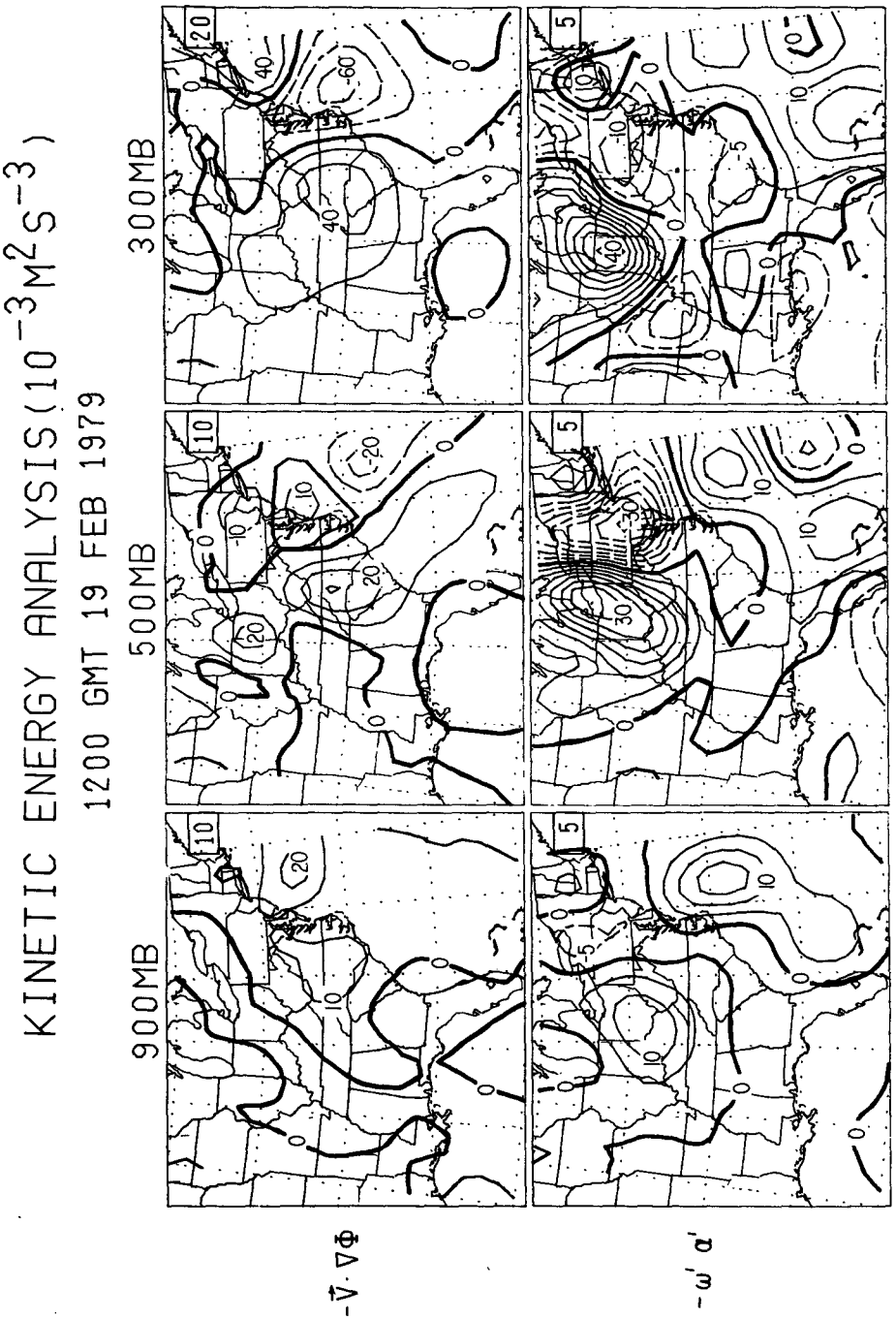

FIG. 13. As in Fig. 12 except for 1200 GMT 19 February 1979.

residuals tend to maximize in the anticyclonic shear region (area 4) south of the main trough to the north. The error bounds given by Smith (1980) suggest that the average values of the flux, generation and residual terms are well above typical uncertainty estimates and that a subgrid-scale energy exchange is probably present.

The kinetic energy structure of the Presidents' Day storm does not match the overall cyclone composite of Kung and Baker (1975) or the summary of individual cyclone events by Smith (1980). A positive residual is demanded in the present case in order to help the generation term counterbalance the strong horizontal export of kinetic energy away from the storm environment. Apparently, the subsynoptic-scale nature of the cyclogenetic event known as the Presidents' Day storm is associated with a variety of physical processes that are not truly represented by synoptic-scale variables.

7. Oceanic sensible and latent heat fluxes

Figure 14 shows the sensible and latent heat fluxes for the 36 h period ending 1200 GMT 19 February. The fluxes were computed from the bulk aerodynamic formulas with an exchange coefficient of 1.6×10^{-3} on a 1° latitude–longitude mesh. A gridded sea surface temperature analysis was tabulated from the composite analysis presented in Bosart (1981). The most interesting result is that fluxes maximize in the flow of previously very cold, continental air that is now moving *westward* toward the coast *prior* to incipient coastal frontogenesis. Cyclogenesis along the coastal front occurs to the west of the locus of maximum sensible and latent heat flux and involves surface inflow air that has been subjected to considerable warming and moistening. The latent heat flux is roughly three times the sensible heat flux.

These fluxes, while not as dramatic as those reported by Ichiye and Zipser (1967) or Gall and Johnson (1971) for outbreaks of cold arctic air in the wake of intense western Atlantic cyclogenesis, are certainly representative of the composite conditions described by Petterssen *et al.* (1962) occurring in the wake of Atlantic cyclones. The crucial difference, however, is that the fluxes documented here occur in conjunction with an *onshore* flow of previously well chilled arctic air. Prior to the onset of the onshore flow regime a broad but intense east–west oriented baroclinic zone prevailed over the United States east of the Rockies with a southern extent in lower Florida. A region of enhanced baroclinicity was then created along a line parallel to the Carolina coast in response to differential heating and moistening, and probably was reinforced by differential roughness and cold air damming.

The quasi-geostrophic 1000 mb height tendency due to sensible heating alone in the 1000–850 mb layer (see Boyle and Bosart, 1983) is shown in Fig. 15. Height falls exceeding 80 m $(12\ \text{h})^{-1}$ occur in a narrow zone parallel to the coast *prior* to and during coastal frontogenesis (0000 and 1200 GMT 18 February). These height falls maximize to the north and east of the incipient cyclone in the 12 h period ending 0000 GMT 19 February. By 1200 GMT 19 February the quasi-geostrophic height tendency contribution due to sensible heating is zero in the vicinity of the rapidly developing cyclone and is large in the wake of the cyclone as cold air moving offshore is heated from below (Fig. 14). We hypothesize that the sensible heat flux helps to condition the precyclogenetic environment by enhancing the lower tropospheric coastal baroclinic zone. This is favorable to frontogenesis and cyclogenesis as warm air advection is then more effective in generating cyclonic vorticity by convergence near the surface.

8. Surface frontogenesis

Frontogenesis computations for the 36 h period ending 1200 GMT 19 February are illustrated in Fig. 16. Observed wind frontogenesis was computed according to

$$\frac{d}{dt}|\nabla\theta| = \frac{1}{2}|\nabla\theta|\left\{\left(\frac{\partial u}{\partial x} - \frac{\partial u}{\partial y}\right)\sec 2a \cos 2b - \nabla \cdot \mathbf{V}_h\right\}, \tag{7}$$

where a is the angle between the x-axis and the axis of dilatation and b the angle between an isentrope and the axis of dilatation. All calculations were performed using procedures described by Bosart (1975) on a 1° latitude–longitude mesh. According to (7), deformation of the wind (first term on the right-hand side) will be frontogenetical whenever the angle between the isotherms and the axis of dilatation is less than 45 deg. Geostrophic frontogenesis was calculated according to the procedure given by Saucier (1955).

A locus of observed wind frontogenesis is seen parallel to the coast at 1200 GMT 18 February in Fig. 16. Peak values reach 3° $(100\ \text{km})^{-1}$ $(3\ \text{h})^{-1}$ at the time of incipient coastal frontogenesis. The frontogenesis is driven by convergence and deformation associated with the *ageostrophic* part of the wind (not shown). Meanwhile, the geostrophic part of the flow contributes *frontolytically* along the Georgia–South Carolina coast. This pattern continues in the following 12 h and it is only by 1200 GMT 19 February, coincident with the onset of rapid cyclogenesis, that the geostrophic and observed wind frontogenesis rates are frontogenetical along the mid-Atlantic coast. Fi-

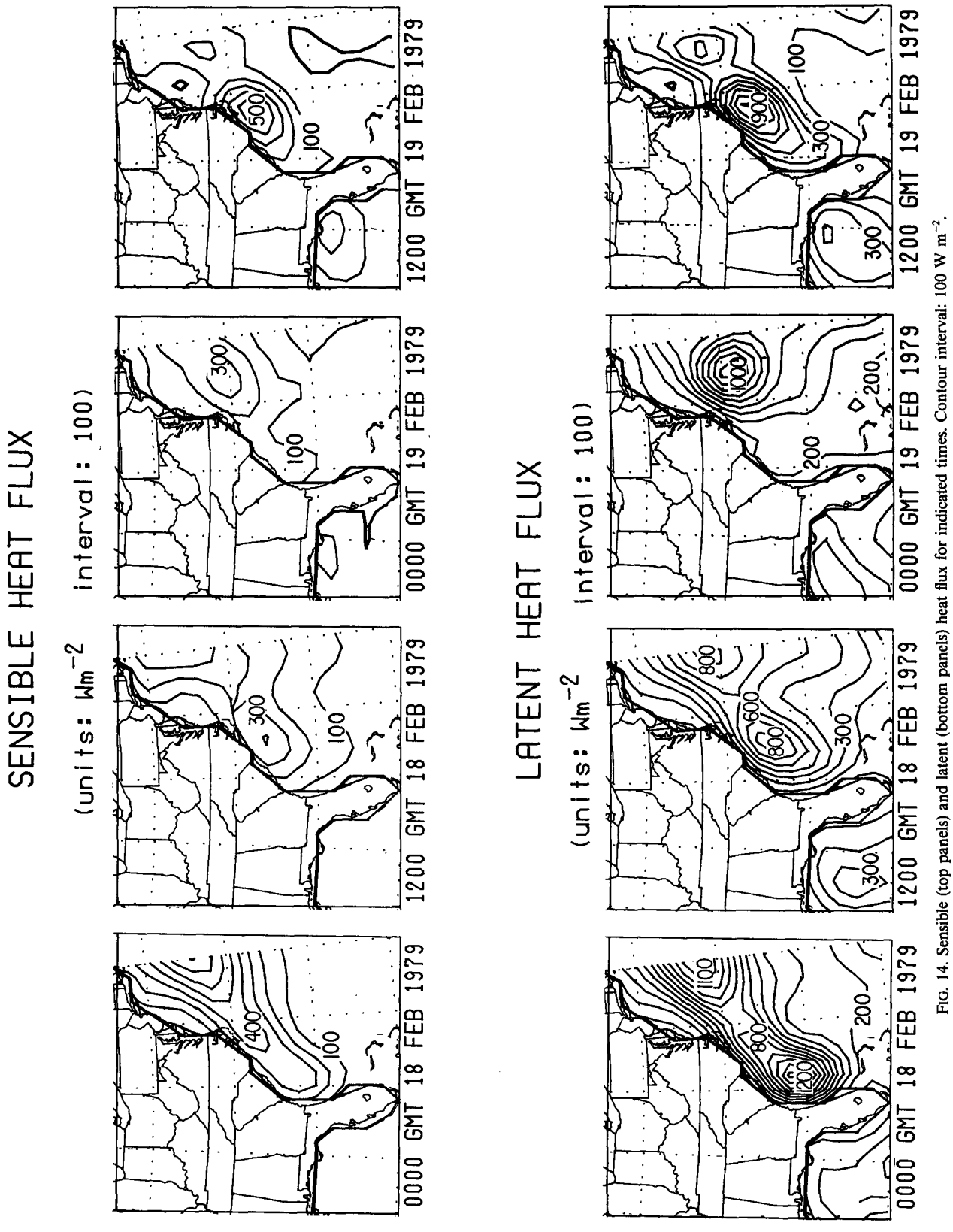

FIG. 14. Sensible (top panels) and latent (bottom panels) heat flux for indicated times. Contour interval: 100 W m^{-2}.

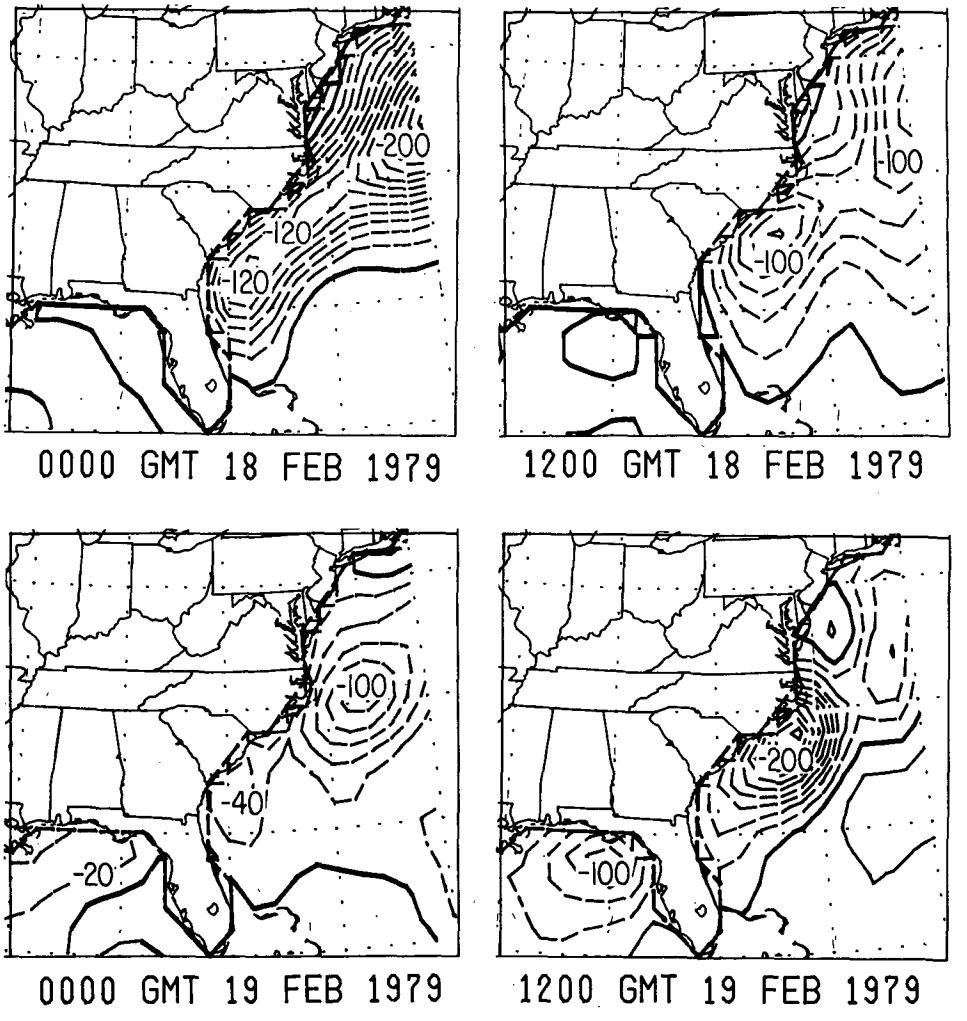

FIG. 15. Computed quasi-geostrophic 1000 mb height tendency due to sensible heating at the indicated times. Contour intervals: 20 m (12 h)$^{-1}$.

nally, Fig. 17 depicts the observed wind frontogenesis due to sensible heating computed according to $\nabla\theta \cdot \nabla(d\theta/dt)/|\nabla\theta|$. A frontogenesis rate of nearly 1°C (100 km)$^{-1}$ (3 h)$^{-1}$ just offshore is indicated through 0000 GMT 19 February.

Clearly frontogenetical processes (Figs. 16 and 17) maximize in this coastal zone with differential diabatic heating due to sensible heating contributing to 30–40% of the frontogenesis rate. Although the synoptic-scale flow is initially frontolytical, it is very important in allowing air parcels modified by an over water trajectory to come into juxtaposition with unmodified continental air flowing southwestward along the coastal zone. This process helps to enhance the "background" baroclinicity and preconditions the atmosphere for a subsynoptic-scale response once warm air advection begins in the lower troposphere. The presence of a coastline helps to anchor surface convergence and cyclonic vorticity production that accompanies frontogenesis and shallow cyclogenesis.

9. Transverse vertical circulations

We now discuss the semigeostrophic vertical circulations associated with the Presidents' Day storm in order to help increase our physical understanding of the cyclogenesis process. Sawyer (1956), Eliassen (1962) and Shapiro (1981) have employed the semigeostrophic momentum approximation to derive transverse secondary frontal circulations under the assumption of Boussinesq flow and the neglect of along-front ageostrophic advections. Despite the fact that Uccellini *et al.* (1984) have shown that the geostrophic momentum approximation broke down as the flow was becoming "less balanced" near the ridge crest, we will proceed cautiously and use the

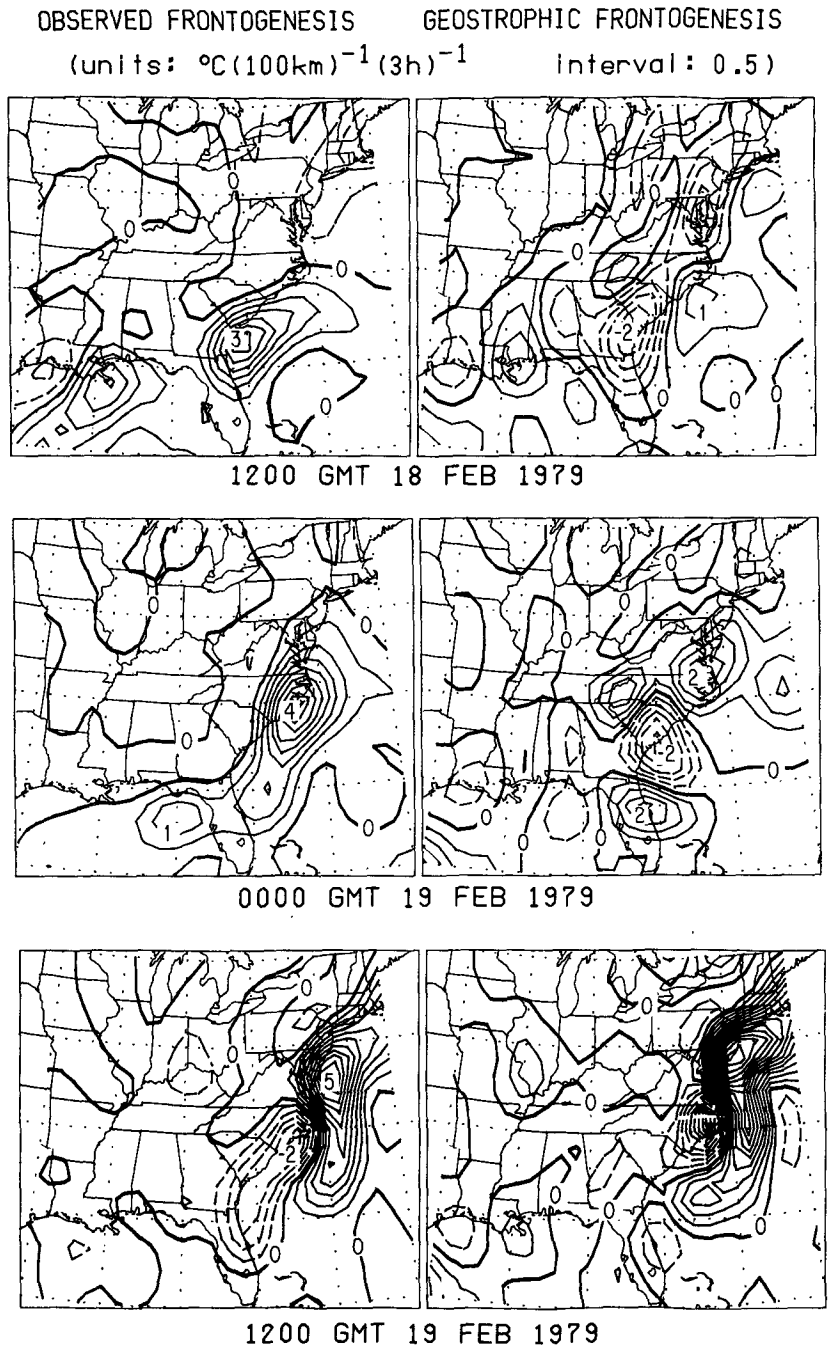

FIG. 16. Frontogenesis computed from the observed winds (top panels) and geostrophically (bottom panels) for the given times. Zero contour (heavy solid lines) with frontogenesis (frontolysis) given by thin solid (thin dashed) lines. Contour interval: 0.5°C (100 km)$^{-1}$ (3 h)$^{-1}$.

semigeostrophic equations. Bluestein and Thomas (1984) have presented evidence that the use of the geostrophic momentum approximation leads to a reasonable qualitative explanation of the ageostrophic circulation in regions of appreciable curvature, whereas quasi-geostrophic theory does not. Hoskins and Draghici (1977) presented the three-dimensional version of Eliassen's (1962) cross-frontal circulation as follows:

$$\frac{\partial}{\partial X}\left(q_g \frac{\partial \psi_1}{\partial X}\right) + f^2 \frac{\partial^2 \psi_1}{\partial Z^2} = 2Q_{s1} - \frac{\partial}{\partial X}\left(q_g \frac{\partial \psi_2}{\partial Y}\right), \quad (8)$$

$$\frac{\partial}{\partial Y}\left(q_g \frac{\partial \psi_2}{\partial Y}\right) + f^2 \frac{\partial^2 \psi_2}{\partial Z^2} = 2Q_{s2} - \frac{\partial}{\partial Y}\left(q_g \frac{\partial \psi_1}{\partial X}\right), \quad (9)$$

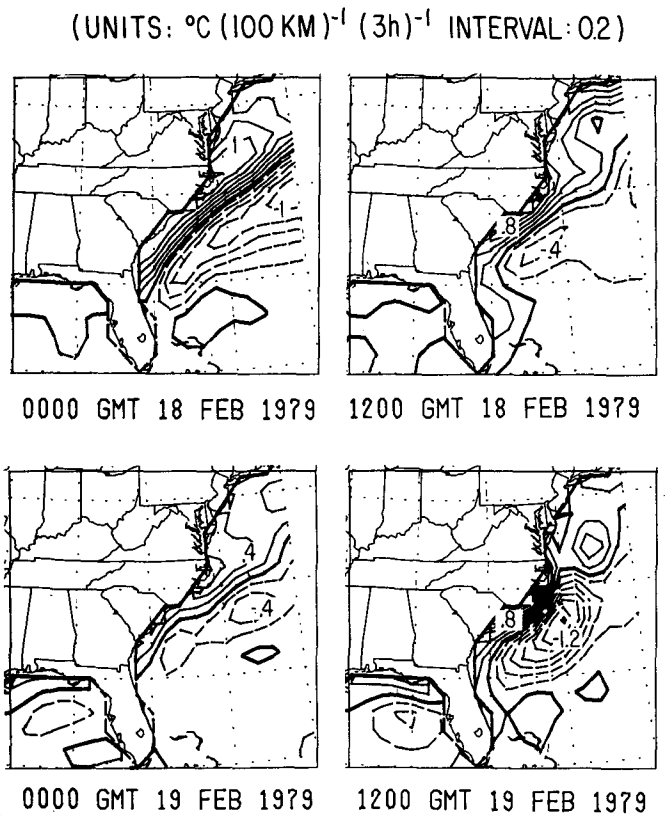

FIG. 17. Frontogenesis due to sensible heating. Contours and units as in Fig. 16 except 0.2°C (100 km)$^{-1}$ (3 h)$^{-1}$ interval.

where

$$u_{ag}^* = -\partial\psi_1/\partial Z = u_{ag} + \frac{w}{f^2}\frac{\partial^2\Phi^*}{\partial X \partial Z}$$

$$v_{ag}^* = -\partial\psi_2/\partial Z = v_{ag} + \frac{w}{f^2}\frac{\partial^2\Phi^*}{\partial Y \partial Z}$$

$$Q_{s1} = -\frac{g}{\theta_0}\frac{\partial u_g}{\partial X}\frac{\partial \theta}{\partial X} - \frac{g}{\theta_0}\frac{\partial v_g}{\partial X}\frac{\partial \theta}{\partial Y}$$

$$Q_{s2} = -\frac{g}{\theta_0}\frac{\partial u_g}{\partial Y}\frac{\partial \theta}{\partial X} - \frac{g}{\theta_0}\frac{\partial v_g}{\partial Y}\frac{\partial \theta}{\partial Y}$$

$$w^* = \partial\psi_1/\partial X + \partial\psi_2/\partial Y = w/J$$

$$\Phi^* = \Phi + \tfrac{1}{2}(u_g^2 + v_g^2)$$

Hoskins and Draghici (1977) further pointed out that the linkage terms involving ψ_1 and ψ_2 on the right-hand side of (8) and (9) will be negligible only under conditions when the geostrophic length scale along the respective axes dominates the Rossby radius of deformation. In this case (8) and (9) reduce to Eliassen's cross-frontal circulation equation. The retention of the linkage terms then represents a natural extension of Eliassen's computation to a three-dimensional domain for any arbitrary circulation. The solution of (8) and (9) is obtained via an iterative technique. By first assuming $\psi_2 = 0$ in (8), one can solve for ψ_1 on each discrete XZ plane, then substitute ψ_1 in the right-hand side of (9) and solve for ψ_2 on each discrete YZ plane. This procedure is repeated until the differences of ψ_1 and ψ_2 between two consecutive iterations is within a preassigned tolerance.

The resulting vertical motion field is displayed in cross section format in Fig. 18, while the individual forcing functions and their sum appear for the same longitudinal cross sections in Fig. 19. A careful comparison of Figs. 3 and 18 discloses that the semigeostrophic vertical motions are underestimated in Fig. 18 relative to Fig. 3. The difference is probably artificial and is likely to be a reflection of the limited domain and choice of boundary condition ($\psi = 0$) in the solution of (8) and (9). Despite some significant discrepancies with the kinematic vertical motions shown in Fig. 2, the sense of the semigeostrophic vertical motions is qualitatively reasonable and we proceed accordingly. Figure 18 shows that the vertical motions become more vigorous with time, with the

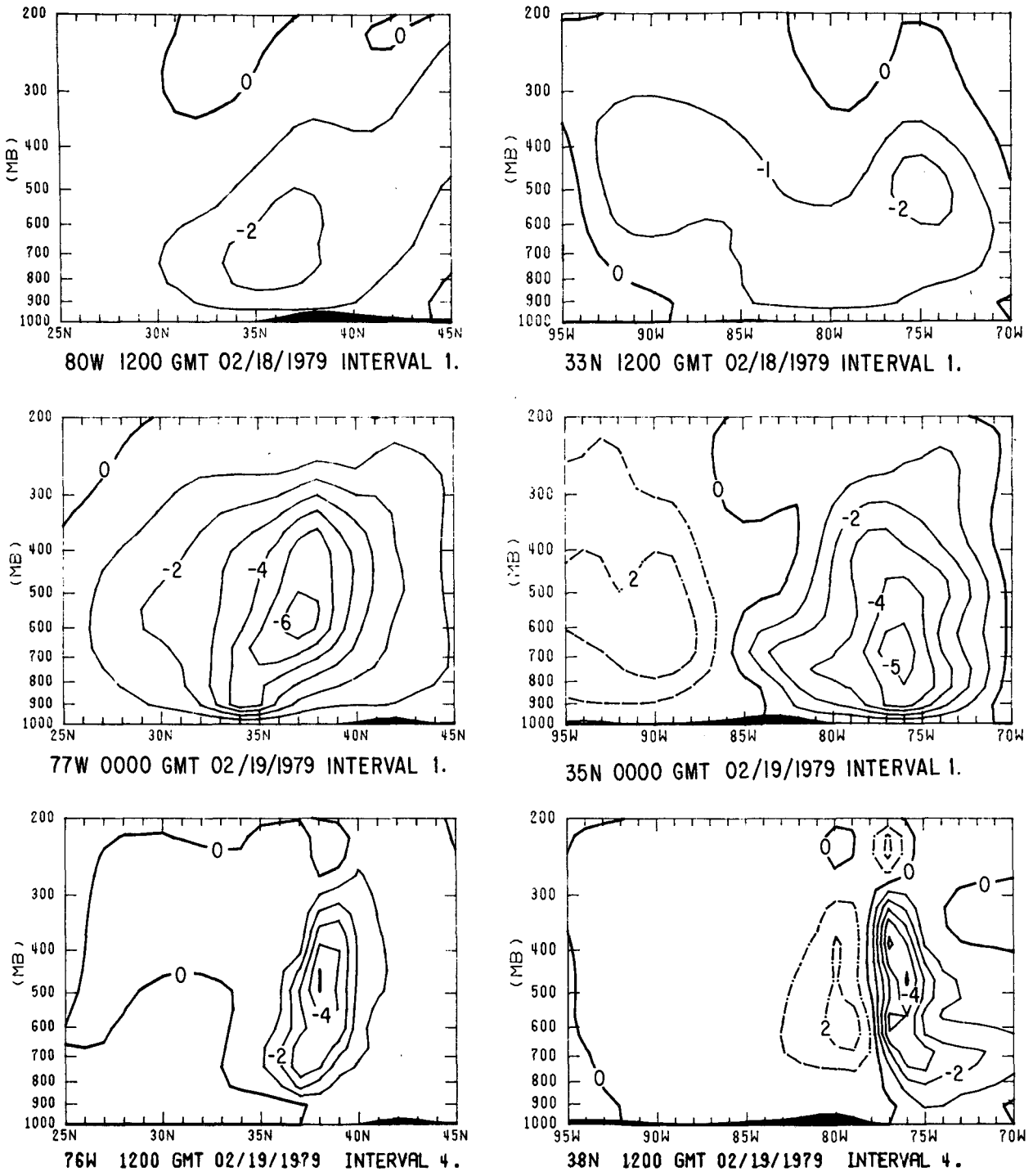

FIG. 18. Cross sections of semigeostrophic vertical motions (10^{-3} mb s^{-1}) along selected longitudes and latitudes for 1200 GMT 18 February through 1200 GMT 19 February 1979. Zero vertical motion, ascent and descent are indicated by heavy solid, thin solid and thin dashed lines, respectively. Contour interval is given below lower right corner of each panel.

level of maximum ascent along the coast rising gradually from 700 to 500 mb as the initially shallow cyclogenesis intensifies and expands upward.

The *YP* cross section forcing functions displayed in Fig. 19 include the breakdown of the $2Q_{s2}$ term into contributions from confluence and shear (anal-

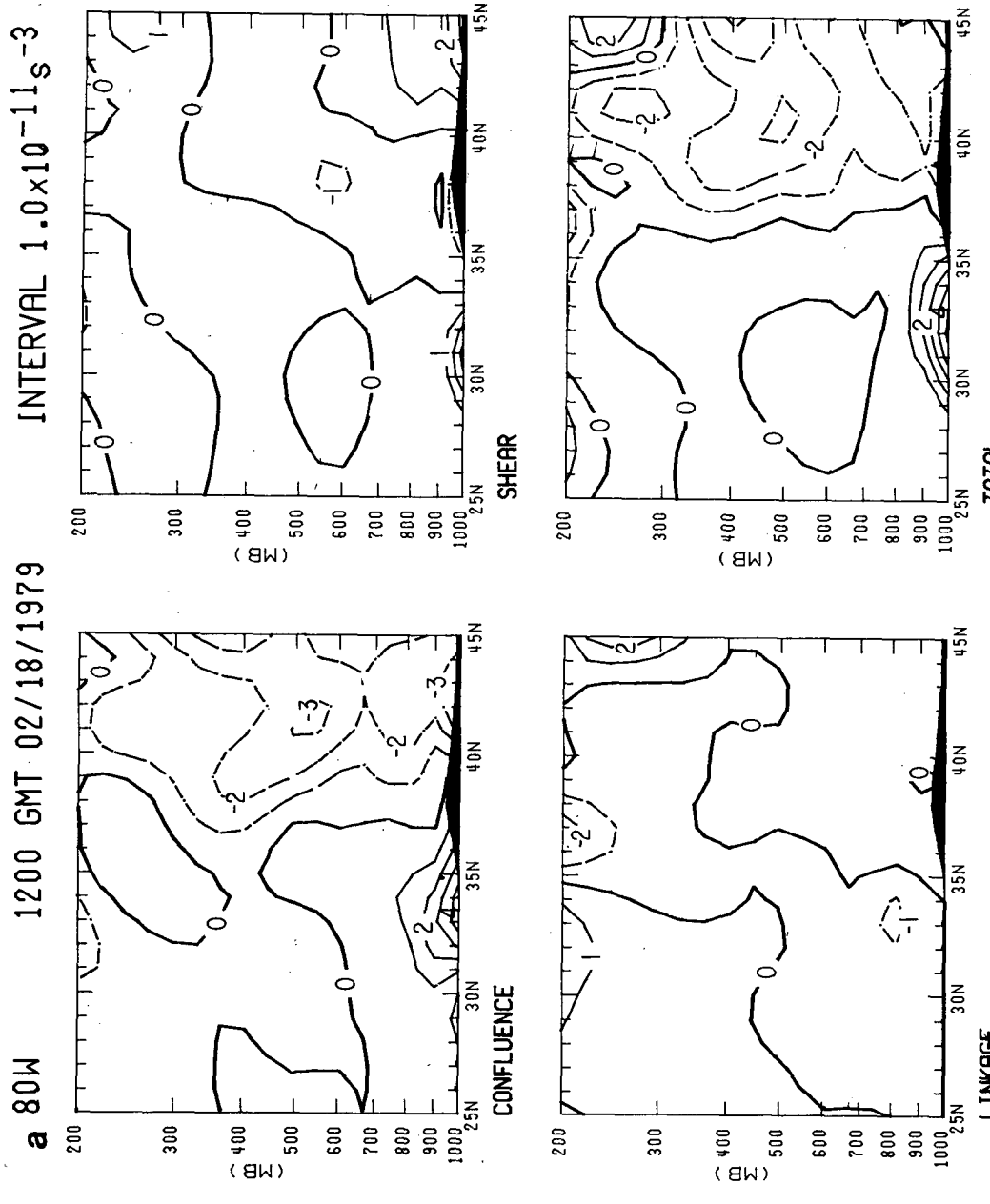

FIG. 19. Longitudinal cross sections of forcing functions on the right-hand side of Eq. (9), including confluence $[(-g/\theta_0)(\partial v_g/\partial Y)(\partial\theta/\partial Y)]$ and shear $[(-g/\theta_0)(\partial u_g/\partial Y)(\partial\theta/\partial X)]$ parts of $2Q_{22}$, linkage term and their sum for (a) 1200 GMT 18 February, (b) 0000 GMT 19 February and (c) 1200 GMT 19 February 1979. Zero contour (heavy solid lines) with positive (negative) values denoted by thin solid (dashed) lines. Longitude and contour interval as indicated.

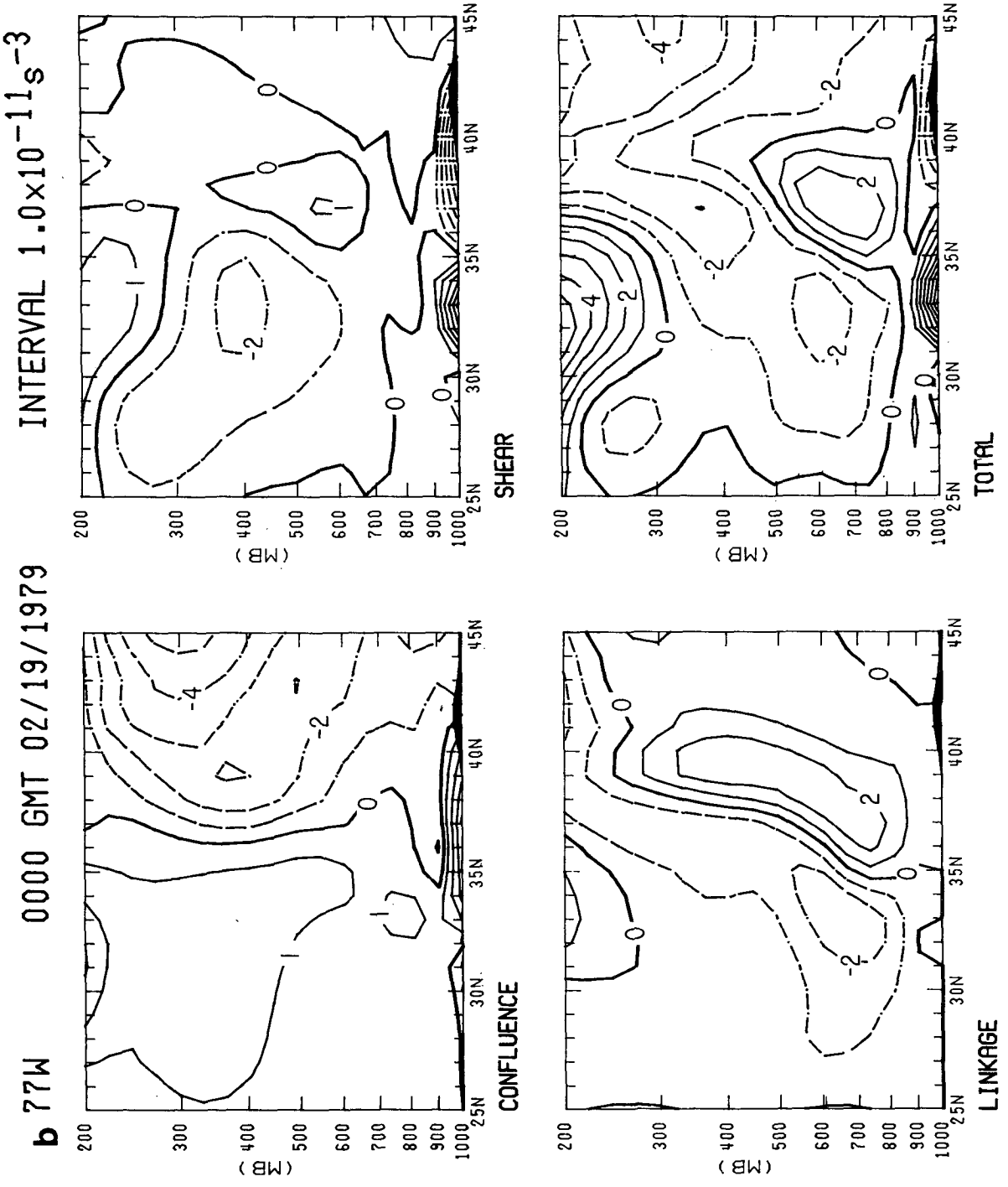

FIG. 19. (*Continued*)

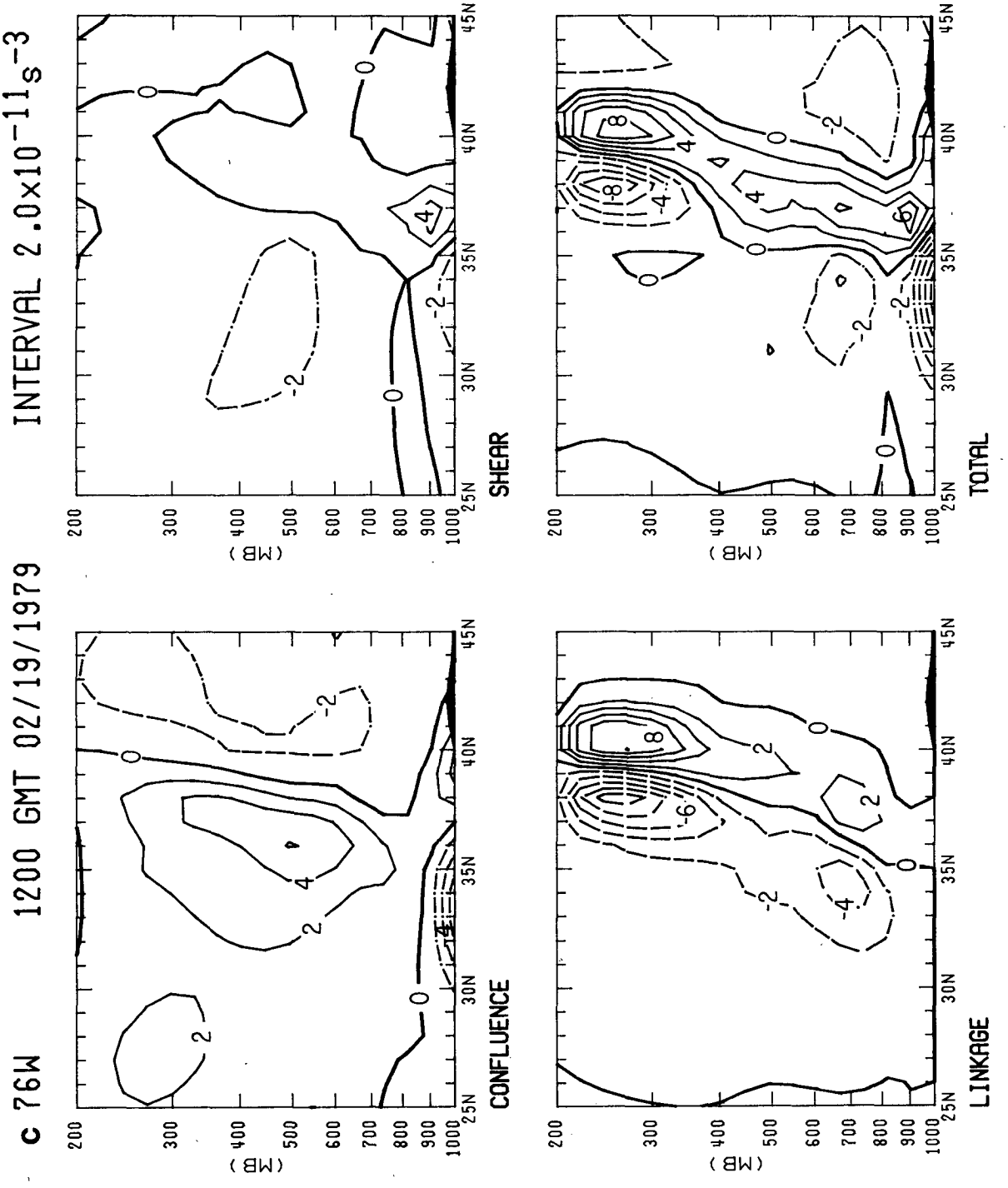

FIG. 19. *(Continued)*

ogous to stretching and shearing deformation effects). The sense of the implied circulation is counterclockwise (clockwise) about maximum (minimum) and is denoted by solid (dashed) contours. Confluence dominates the lower troposphere along 80°W at 1200 GMT 18 February, as coastal frontogenesis proceeds as surface winds are tending to blow perpendicular to the frontal boundary. The absence of an appreciable forcing function in the upper troposphere may be an artifact of the cross section choice. Uccellini *et al.* (1984) show that the 225 mb divergence (their Fig. 13) maximizes along 85°W. The linkage term (a measure of the suitability of neglecting along flow accelerations) is significant near the crest of the subtropical jet stream in the upper troposphere.

By 0000 GMT 19 February the confluence and shearing forcing functions are more equal and maximize in the midtroposphere. This implies a vigorous boundary layer circulation, which is not properly reflected in Fig. 18 because of the computational method and choice of a lower boundary condition. The linkage term is now quite important in the 800–300 mb layer. We conclude that any two-dimensionality assumption for the circulation in a plane is questionable for the present case. This confirms a conclusion of Uccellini *et al.* (1984) that the semigeostrophic momentum approximation was violated in the ridge at jet level at 1200 GMT 18 February. Similarly, the results of Shapiro and Kennedy (1981) suggest a similar problem in the tightly curved cyclonic flow near the coast 24 h later.

Finally, by 1200 GMT 19 February we see a vigorous forcing function with confluence and shear effects mostly in phase (out of phase) near the ground (aloft) such that the dominant forcing remains anchored to the surface with a secondary maximum in the midtroposphere. The linkage term, which is now comparable to the other terms in the midtroposphere, dominates the upper troposphere and is indicative of the fully three-dimensional nature of the circulation. Cross sections at other latitudes and longitudes (not shown) support this description. We conclude that the vigor of the near surface forcing functions can be viewed as additional evidence for the importance of boundary layer processes to cyclogenesis in this case. We speculate that the inclusion of diabatic forcing would strengthen this conclusion.

10. Summary and conclusions

A comparison of kinematic, quasi-geostrophic and semigeostrophic vertical motions for the Presidents' Day cyclone reveals that the kinematic method better captures the lower tropospheric ascent maximum along the coast in the precyclogenetic storm environment. This is related to the highly ageostrophic nature of the boundary layer flow accompanying coastal frontogenesis. As cyclogenesis proceeds, the three vertical motion methods come into better agreement. The semigeostrophic vertical motions, however, are superior to the quasi-geostrophic vertical motions in that the ascent–descent dipole is better defined and shows a vertical tilt in better agreement with observation.

The semigeostrophic vertical motions appear to be quantitatively deficient in the ridge region where the flow is unbalanced (Uccellini *et al.*, 1984) and in the area of strong cyclonic curvature (Shapiro and Kennedy, 1981). The problem appears to be particularly acute in the calculation of the full three-dimensional semigeostrophic circulation forcing functions after Hoskins and Draghici (1977), although a portion of the discrepancy can be attributed to the computational method and the choice of a lower boundary condition. Qualitatively, however, the semigeostrophic vertical motions correspond reasonably well to the observed weather in the region of strong cyclonic curvature in agreement with the results of Bluestein and Thomas (1984).

An analysis of the moisture budget shows that the moisture flux convergence in the surface to 700 mb layer expands eastward to the coast and intensifies as coastal frontogenesis commences. Convergence in the presence of water vapor dominates horizontal advection in the coastal boundary layer, from which it was deduced that ageostrophic motions are crucial in providing *in situ* moisture for precipitation development.

The kinetic energy results disclose that a significant positive residual is necessary to support generation of kinetic energy by cross contour flow to offset the horizontal flux divergence of kinetic energy away from the storm environment. Important contributions to the generation of kinetic energy are made both by the divergent and nondivergent wind. Barotropic processes are more important in generating kinetic energy in the storm environment, whereas baroclinic processes dominate the immediate storm area.

The vorticity analysis reveals that lower tropospheric vorticity increases primarily by convergence in the incipient cyclogenetic environment. Cyclonic vorticity advection in the mid and upper troposphere in the vicinity of the developing storm is minimal. The vertical advection of vorticity, however, is important in the midtroposphere 12 h after the initial growth of vorticity in the lower troposphere. This suggests that the initial storm development was significantly influenced by lower tropospheric processes. The ensuing rapid storm spinup following the onset of pronounced cyclonic vorticity advection aloft is then aided by a preexisting area of cyclonic vorticity in the lower troposphere in which marked convergence develops. The rapid cyclogenesis stage is also marked by the approach of a semigeostrophic potential

vorticity maximum in the mid and upper troposphere, as first noted by Uccellini *et al.* (1984, 1985). Development occurs accompanying the stretching of vortex tubes as this maximum approaches the cold side of the storm. Considerable growth of boundary layer semigeostrophic potential vorticity occurs *in situ* with coastal frontogenesis prior to the rapid cyclone intensification stage. This low-level maximum is located just to the northwest of the deepening storm.

An analysis of the oceanic sensible and latent heat fluxes shows that planetary boundary layer processes are vital to the incipient storm development in the *onshore* flow *prior* to coastal front development. The observed wind field is strongly frontogenetical as coastal frontogenesis commences, whereas the geostrophic flow is frontolytical. This reinforces the importance of ageostrophic processes in the prestorm boundary layer in setting the stage for later cyclogenesis.

Uccellini *et al.* (1984) showed that unbalanced flow in the subtropical jet as 1200 GMT 18 February resulted in a coupled indirect vertical circulation near the Atlantic coast. They indicated that the low-level jet in the lower branch of this circulation aided the development of heavy snow in the southeastern United States even though the trough axis was located well upstream. Our results attest to the importance of planetary boundary layer processes and cold air damming to the east of the Appalachians in providing a ripe precyclogenetic environment along the coast. We hypothesize that these processes contributed significantly to the relative uniqueness of the intensity of the Presidents' Day storm by providing a locus of frontogenesis and cyclonic vorticity generation parallel to the coast. This allowed a shallow, developing cyclone to propagate north-northeastward into a more favorable environment for explosive deepening with the approach of a potent short wave trough aloft from the Ohio Valley.

Our work, in conjunction with that of Uccellini *et al.* (1984, 1985), on this storm points to the need for considering East Coast cyclogenesis as a scale interaction problem. We are excited at the prospect of obtaining data sets to accomplish this task from the upcoming Genesis of Atlantic Lows Experiment (GALE) to be conducted in the southeastern United States between 15 January and 15 March 1986.

Acknowledgments. This manuscript has benefited from the thoughtful comments of Howie Bluestein, John Gyakum, Steve Silberberg and the anonymous referees. Louis Uccellini's persistence in getting us to see beyond the boundary layer is greatly appreciated. Ms. Cynthia Erdt and Ms. Kathy Stutsrim provided capable editorial assistance and Ms. Marilyn Peacock provided help with figure preparation. The research was supported by NSF Grant ATM802655702.

APPENDIX

List of Symbols

c_p	specific heat at constant pressure
f	Coriolis parameter
g	gravity
h	$(R/p)(p/p_0)^\kappa$
J	Jacobian of the transformation
$\mathbf{k}$	unit vector in the vertical
p	pressure
p_0	surface pressure
Q_g	quasi-geostrophic Q-vector
Q_s	semigeostrophic Q-vector
Q_{s1}	X-component of semigeostrophic Q-vector
Q_{s2}	Y-component of semigeostrophic Q-vector
q	specific humidity
R	gas constant for dry air
u_{ag}	zonal component of ageostrophic wind
u_g	zonal component of geostrophic wind
$\mathbf{V}$	horizontal wind vector
$\mathbf{V}_D$	horizontal divergent wind vector
$\mathbf{V}_g$	horizontal geostrophic wind vector
v_{ag}	meridional component of ageostrophic wind
v_g	meridional component of geostrophic wind
$\mathbf{V}_R$	horizontal nondivergent wind vector
w	vertical motion in height coordinates
z	geometric height
α	specific volume
Φ	geopotential (gz)
κ	R/c_p
θ	potential temperature
θ_0	constant reference potential temperature
σ	static stability $(-h\partial\theta/\partial p)$
ω	vertical motion in pressure coordinates
ψ_1	circulation streamfunction in the semigeostrophic (X, Z) plane
ψ_2	circulation streamfunction in the semigeostrophic (Y, Z) plane
ζ	relative vorticity
ζ_g	geostrophic relative vorticity
∇	two-dimensional del operator in physical (x, y) space
∇_x	two-dimensional del operator in semigeostrophic (X, Y) space

REFERENCES

Arnason, G., and L. P. Carstensen, 1959: The effects of vertical vorticity advection and turning of vortex tubes in hemispheric forecasts with a two-level model. *Mon. Wea. Rev.*, **87**, 119–127.

Bleck, R., 1973: Numerical forecasting experiments based on the conservation of potential vorticity on isentropic surfaces. *J. Appl. Meteor.*, **12**, 737–752.

——, 1974: Short-range prediction in isentropic coordinates with filtered and unfiltered numerical models. *Mon. Wea. Rev.*, **102**, 813–829.

Bluestein, H. B., and K. W. Thomas, 1984: Diagnosis of a jet streak in the vicinity of a severe weather outbreak in the Texas panhandle. *Mon. Wea. Rev.*, **112**, 2501–2522.

Bosart, L. F., 1975: New England coastal frontogenesis. *Quart J. Roy. Meteor. Soc.*, **101**, 957–978.

——, 1981: The Presidents' Day snowstorm of 18–19 February 1979: A subsynoptic-scale event. *Mon. Wea. Rev.*, **109**, 1542–1566.

Boyle, J. S., and L. F. Bosart, 1983: A cyclone/anticyclone couplet over North America: An example of anticyclone evolution. *Mon. Wea. Rev.*, **111**, 1025–1045.

Carlson, T. B., 1980: Airflow through midlatitude cyclones and the comma cloud pattern. *Mon. Wea. Rev.*, **108**, 1498–1509.

Chen, T.-G., and L. F. Bosart, 1979: A quasi-Lagrangian vorticity budget of composite cyclone–anticyclone couplets accompanying North American polar air outbreaks. *J. Atmos. Sci.*, **36**, 185–194.

——, J. C. Alpert and T. W. Schlatter, 1978: The effects of divergent and nondivergent winds on the kinetic energy budget of a midlatitude cyclone: A case study. *Mon. Wea. Rev.*, **106**, 458–468.

Cressman, G. P., 1961: A diagnostic study of midtropospheric development. *Mon. Wea. Rev.*, **89**, 74–82.

DiMego, G. J., and L. F. Bosart, 1982a: The transformation of Tropical Storm Agnes into an extratropical cyclone. Part I: The observed field and vertical motion computations. *Mon. Wea. Rev.*, **110**, 385–411.

——, and ——, 1982b: The transformation of Tropical Storm Agnes into an extratropical cyclone. Part II: Moisture, vorticity and kinetic energy budgets. *Mon. Wea. Rev.*, **110**, 412–433.

Eliassen, A., 1962: On the vertical circulation in frontal zones. *Geofys. Publ.*, (V. Bjerknes Memorial Vol.) **24**(4), 147–160.

Gall, R. L., and D. R. Johnson, 1971: The generation of available potential energy by sensible heating: A case study. *Tellus*, **21**, 465–482.

Gyakum, J. R., 1983a: On the evolution of the *QE II* storm. Part I: Synoptic aspects. *Mon. Wea. Rev.*, **111**, 1137–1155.

——, 1983b: On the evolution of the *QE II* storm. Part II: Dynamic and thermodynamic structure. *Mon. Wea. Rev.*, **111**, 1156–1173.

Hoskins, B. J., and I. Draghici, 1977: The forcing of geostrophic motion according to the semi-geostrophic equations in an isentropic coordinate model. *J. Atmos. Sci.*, **34**, 1859–1867.

——, and M. A. Pedder, 1980: The diagnosis of middle latitude synoptic development. *Quart. J. Roy. Meteor. Soc.*, **106**, 707–719.

——, I. Draghici and H. C. Davies, 1978: A new look at the ω-equation. *Quart. J. Roy. Meteor. Soc.*, **104**, 31–38.

Ichiye, T., and E. J. Zipser, 1967: An example of heat transfer at the air–sea boundary over the Gulf Stream during a cold air outbreak. *J. Meteor. Soc. Japan*, **45**, 261–270.

Krishnamurti, T. N., 1968: A study of a developing wave cyclone. *Mon. Wea. Rev.*, **96**, 208–217.

Kung, E. C., and W. E. Baker, 1975: Energy transformations in middle latitude disturbances. *Quart. J. Roy. Meteor. Soc.*, **101**, 783–816.

O'Brien, J. J., 1970: Alternative solutions to the classical vertical velocity problem. *J. Appl. Meteor.*, **9**, 197–203.

Pagnotti, V., and L. F. Bosart, 1984: Comparative diagnostic case study of east coast secondary cyclogenesis under weak versus strong synoptic-scale forcing. *Mon. Wea. Rev.*, **112**, 5–30.

Pearce, R. P., 1974: The design and interpretation of diagnostic studies of synoptic-scale atmospheric systems. *Quart. J. Roy. Meteor. Soc.*, **100**, 265–285.

Pedder, M. A., 1981: On the errors of kinematic vertical motion estimation using divergence bias adjustment procedures. *Mon. Wea. Rev.*, **109**, 1813–1816.

Petterssen, S., 1955: A general survey of factors influencing development at sea level. *J. Meteor.*, **12**, 36–42.

——, and S. J. Smebye, 1971: On the development of extratropical storms. *Quart. J. Roy. Meteor. Soc.*, **97**, 457–482.

——, D. L. Bradbury and K. Pedersen, 1962: The Norwegian cyclone models in relation to heat and cloud sources. *Geofys. Publ.*, **24**(9), 243–280.

Sanders, F., and J. R. Gyakum, 1980: Synoptic dynamic climatology of the bomb. *Mon. Wea. Rev.*, **108**, 1589–1606.

Saucier, W. J., 1955: *Principles of Meteorological Analysis*. University of Chicago Press, 438 pp.

Sawyer, J. S., 1956: The vertical circulation at meteorological fronts and its relation to frontogenesis. *Proc. Roy. Soc. London*, **A234**, 346–362.

Shapiro, M. A., 1981: Frontogenesis and geostrophically forced secondary circulations in the vicinity of jet stream–frontal zone systems. *J. Atmos. Sci.*, **38**, 954–973.

——, and P. J. Kennedy, 1981: Research aircraft measurements of jet stream geostrophic and ageostrophic winds. *J. Atmos. Sci.*, **38**, 2642–2652.

Smith, P. J., 1980: The energetics of extratropical cyclones. *Rev. Geophys. Space Phys.* **18**, 378–386.

——, and C. P. Lin, 1978: A comparison of synoptic-scale vertical motions computed by the kinematic methods and two forms of the omega equation. *Mon. Wea. Rev.*, **106**, 1687–1694.

Tibaldi, S., A. Buzzi and P. Malguzzi, 1980: Orographically induced cyclogenesis: Analysis of numerical experiments. *Mon. Wea. Rev.*, **108**, 1302–1314.

Uccellini, L. F., P. J. Kocin, R. A. Petersen, C. H. Wash and K. F. Brill, 1984: The Presidents' Day cyclone of 18–19 February 1979: Synoptic overview and analysis of the subtropical jet streak influencing the pre-cyclogenetic period. *Mon. Wea. Rev.*, **112**, 31–55.

——, D. Keyser, C. H. Wash and K. F. Brill, 1985: The Presidents' Day cyclone of 18–19 February 1979: Influence of a tropopause fold on rapid cyclogenesis. *Mon. Wea. Rev.*, (In press).